Identification and characterization of novel ligands for human bitter taste receptor T2R7

By

Kun Liu

A Thesis submitted to the Faculty of Graduate Studies of

The University of Manitoba

in partial fulfilment of the requirements of the degree of

MASTER OF SCIENCE

Department of Oral Biology

University of Manitoba

Winnipeg, Canada

Abstract

Humans have five basic taste sensations which are bitter, sweet, umami, salt and sour. Salt and sour are mediated by ion channel-linked receptors, while bitter, sweet and umami are sensed by cell surface G protein-coupled receptors (GPCRs). Among the five basic taste modalities, the bitter taste signaling mechanism is the most complex and least understood. This is in part due to the large number of bitter taste receptors (T2Rs) in humans (n=25), and the wide range of bitter compounds they detect. The T2Rs are expressed in the oral cavity as well as in many extraoral tissues. The activation of T2Rs in the oral cavity elicits bitter taste sensation, while the activation of the extraoral T2Rs causes various physiological and pathophysiological responses. Recent findings showed that T2R activation caused muscle relaxation and bronchodilation of pre-contracted airway smooth muscle. Moreover, bacterial quorum sensing molecules were shown to activate T2Rs in extraoral tissues. In view of the importance of T2R functions in extraoral tissues, it is of great value to study the structure-function relationship of T2Rs and identify efficient ligands.

Hitherto, there have been few studies published involving human bitter taste receptor 7 (T2R7). Only few agonists have been identified for the T2R7 receptor, and no structure-function studies on the T2R7 receptor have been reported. In this study, different compounds including known T2R7 agonists, common bitter compounds, antibiotics and quorum sensing molecules were tested for their ability to activate or inhibit T2R7 heterologously expressed in HEK293T cells. Results suggest that T2R7 is activated by novel ligands including dextromethorphan (DXM), diphenhydramine (DPH), thiamine,

tobramycin and erythromycin. In contrast, beef protein hydrolysates purified by RP-HPLC quenched quinine activated T2R7 signal. This suggests that beef hydrolysates may contain potent T2R7 blockers.

To understand the structure of the ligand binding pocket in T2R7, molecular model guided site-directed mutagenesis was pursued. Eighteen mutants were made at nine amino acid positions in the ligand binding pocket of T2R7 and their expression was characterized by flow cytometry. All of the mutants were properly expressed on the cell surface. Functional characterization of the mutants including intracellular calcium mobilization in response to quinine and DXM treatment allowed mapping of the ligand binding pocket of T2R7. Taken together, this study identified novel ligands for T2R7 and elucidated the important amino acids involved in T2R7 ligand binding.

ACKNOWLEDGEMENTS

First, I extend my sincerest thanks to my supervisor, Dr. Chelikani. During my study, he helped me, supported me in every aspect, encouraged me all the time, and guided me all through my study. Without him, I won't be able to accomplish my study.

I also want to express my gratitude to my committee members, Dr. Raj Bhullar and Dr. Hugo Bergen. The suggestions I received from them during my project are insightful. I also appreciate their valuable suggestions for my thesis writing.

I thank my lab members Raju, Feroz, Nisha and everyone else. Thank you for helping me all the time, teaching me all the techniques and answering all my questions with patience. It was really lucky for me to work with such a friendly group of students who are always ready to help each other.

Last but not least, I extend my deepest thanks to my family and friends. I thank my parents and in-laws for supporting my study with love. I owe my special thanks to my husband, Bennett, who has supported me in both my study and my daily life. I thank my friends Shujun, Gao, Shasha, Xuan, Colin, Seb, Wenyan, and Lin. You guys have made my life warm and colorful.

TABLE OF CONTENTS

LIST OF TABLES

LIST OF FIGURES

LIST OF ABBREVIATIONS

ACE	Angiotensin converting enzyme
Ca^{2+}	Calcium ion
CO_2	Carbon dioxide
DAG	Diacylglycerol
DPH	Diphenhydramine
DXM	Dextromethorphan
ECL	Extracellular loop
ENac	Amiloride sensitive epithelial sodium channel
FACS	Fluorescence-activated cell sorting
FBS	Fetal bovine serum
GDP	Guanosine 5'-diphosphate
GTP	Guanosine 5'-triphosphate
GPCR	G protein-coupled receptor
HEK	Human embryo kidney
ICL	Intracellular loop
IP_3	Inositol triphosphate
Na^+	Sodium ion
NCAM	Neural cell adhesion molecule
PIP_2	Inositol phospholipid
PLC β2	Phospholipase C β2
ROMK	Renal outer medullary potassium channel

TRC	Taste receptor cell
TRPM5	Transient receptor potential cation channel subfamily M member 5
T2R	Bitter taste receptor
TM	Transmembrane
WT	Wild type

CHAPTER 1

INTRODUCTION

1.1 Taste system overview

Humans have five main senses, which are taste (gustation), smell (olfaction), hearing (audition), touch (somatosensation) and vision (sight). Among all these five main sensations, the taste sensation has evolved to enable humans to distinguish between harmful and safe food substances, and to get valuable information about the nutritional contents of food. It is widely accepted that humans can sense five basic tastes, which includes sweet, sour, umami, salt and bitter.

The taste system is constituted of taste buds dispersed on the tongue, soft palate and pharyngeal tissue. Most taste buds are located in papillae distributed on the tongue. In humans, there are three types of papillae containing taste buds, which are fungiform papillae, foliate papillae and vallate papillae, named according to their structure and location (Figure 1) (Barlow 2015). Fungiform papillae are dispersed on the anterior two-thirds of the tongue and are innervated by the facial nerve (chorda tympani branch). Foliate papillae present on two lateral sides of the tongue and are innervated by facial and glossopharyngeal nerves. Vallate papillae lie on the dorsal surface of the posterior part of the tongue and are innervated by glossopharyngeal nerve (Barlow 2015).

1.2 The composition of taste buds

Taste buds are aggregations of two distinct cells, the cells at the base of the buds which are referred to as basal cells, and elongated epithelial cells. The polarized elongated

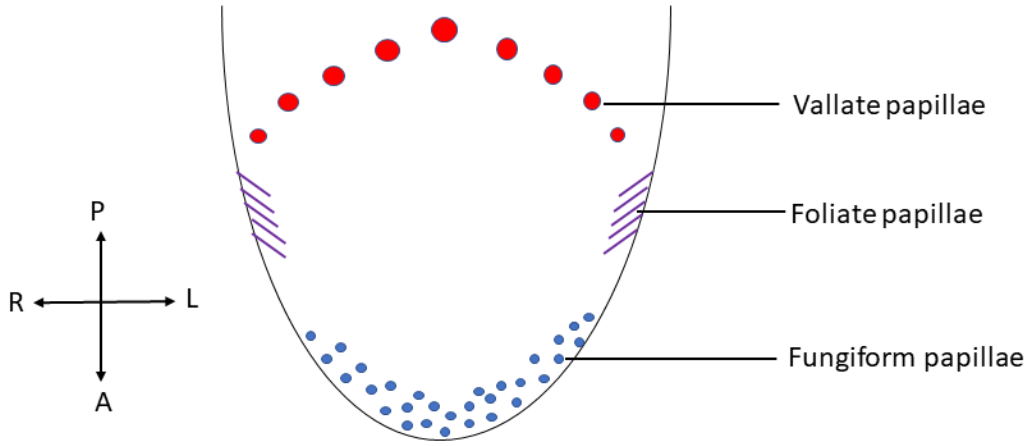

Figure 1 Locations of taste papillae on human tongue. Fungiform papillae are located in the anterior region of the tongue, while foliate papillae lie on the lateral sides of the dorsal surface of the tongue and vallate papillae lie on the posterior section of the tongue. R, right; L, left; P, posterior; A, anterior.

epithelial cells are differentiated cells and are classified into three types: type I cells (dark cells), type II cells (light cells) and type III cells (intermediate cells) (Figure 2) (Finger 2005).

Most of the epithelial cells in the taste bud are type I cells, which are also called dark cells because basophilic dyes accumulate in the cytoplasm. These cells have tall microvilli on their apical side and extended processes encompassing other kind of cells (Lawton 2000). Type I cells express glial glutamate transporter GLAST, membrane-localized ectoATPase called NTPDase2, and renal outer medullary potassium channel (ROMK), suggesting its role as a glial cell (Chaudhari and Roper 2010) .

Type II cells have short microvilli on their apical side in contrast to type I cells. Type II cells express all the components of the taste signaling machinery for bitter, umami and sweet perception (Hoon 1999). These cells thus are the taste receptor-expressing cells (TRCs) for sensing bitter, umami and sweet. However there is no evidence showing that these cells can sense salt and sour (Chaudhari and Roper 2010).

Previous studies have reached a consensus that type III cells are presynaptic cells (Chaudhari and Roper 2010). These cells express several molecules which are related to synaptic connections, including neural cell adhesion molecule (NCAM) (Nelson and Finger 1993), SNAP25 which is a synaptic membrane protein (Yang 2000), and voltage-gated Calcium channel which is related to the release of the neurotransmitters (DeFazio 2006). These cells receive signals from type II cells and form synaptic structures with afferent nerve fibers (Finger 2005).

The basal cells in taste buds are disc-like cells at the base of the taste buds. It was suggested that from these basal cells different types of elongated taste cells may be differentiated (Delay 1986).

1.3 The coding of different tastes

The information of different tastes is transferred to the brain by taste afferent nerve fibers. How the activation of different receptors is interpreted as different tastes in the brain, remains unclear. There are two hypotheses explaining the coding of taste, the labeled line model and the across-fibre model, as represented in Figure 3 (Chandrashekar 2006, Simon 2006, Chaudhari and Roper 2010).

Labeled line model proposes that individual TRCs responds to a single taste modality (bitter, sweet, sour, umami or salty) and are innervated by fibres that deliver the same taste into the central nervous system (Smith and St John 1999), which means each taste is received and transferred by non-overlapping TRCs and nerve fibres (Figure 3 A). In contrast, the across-fibre model purports an overlapped taste transduction pathway. In this model, either each individual TRC is tuned to multiple tastes and the afferent nerve fibres thus are broadly tuned and relay information for several taste modalities (Figure 3 B), or alternatively each individual TRC is tuned to one taste modality only, but afferent nerve fibres carry information for multiple taste modalities (Figure 3 C) (Smith 2000).

1.4 Different taste modalities and their receptors

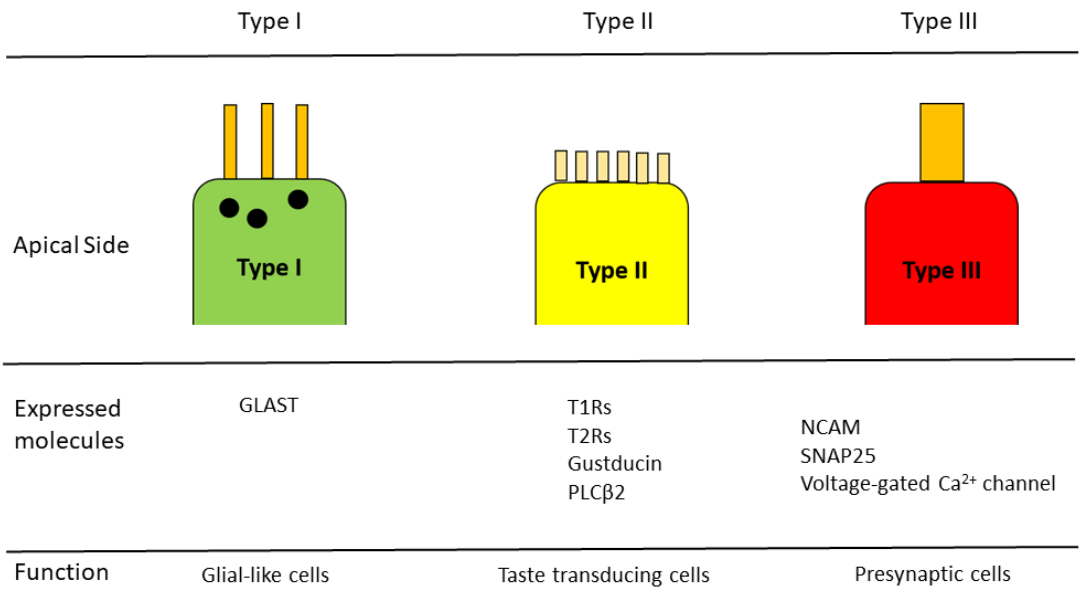

Figure 2 Morphological and physiological characteristics of Type I, Type II and Type III taste cells. Major morphological characteristics of Type I, Type II and Type III taste cells are showed on the top row (left to right). Type I cells have tall microvilli and dark granules on the apical side, while type II cell have short microvilli and type III cells have one tall, thick microvillus. The second row shows different molecules expressed by each cell type, indicating different functions, which are listed in the bottom row.

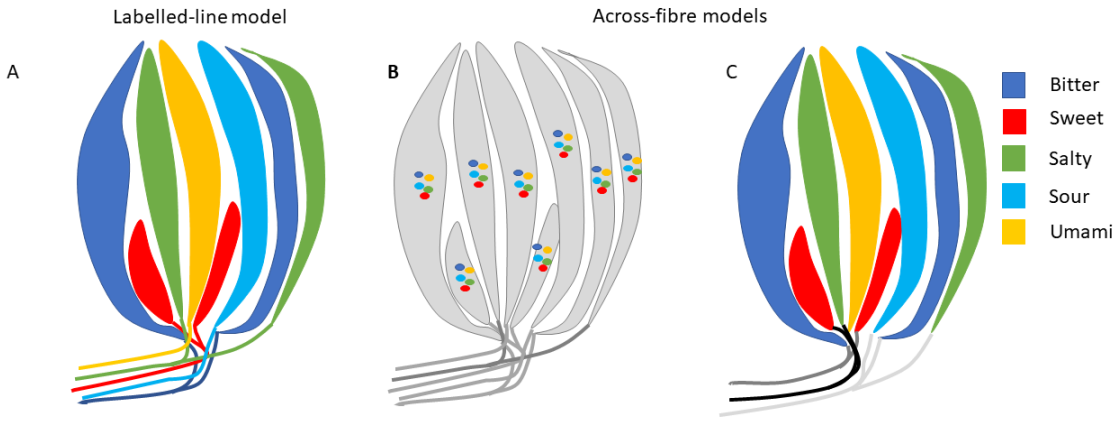

Figure 3 Two models explaining taste encoding. A. Labelled-line model states that each TRC is tuned by one taste modality and is innervated by a nerve fibre, which delivers the same taste. **B and C show two types of across-fibre models. B.** Individual TRCs are tuned to multiple tastes and innervated by afferent nerve fibres, which are also broadly tuned. **C.** Each individual TRC is tuned to one taste modality only but afferent nerve fibres carry information for multiple taste modalities.

A wide variety of compounds are able to activate different taste receptors on TRCs in the oral cavity, which then mediate the taste signal transduction. Salt and sour are transmitted by cation channel-linked receptors, while sweet, umami and bitter are mediated by G protein-coupled receptors (GPCRs) (Figure 4).

(i) Bitter taste

Bitter taste has evolved to help mammals avoid consumption of harmful substances. Humans have innate aversion to bitter food, however, some bitter-tasting food such as coffee, dark chocolate and some fermented foods do not provoke aversion. This can be because humans get tolerant to bitter food with positive effects as the age increases, possibly due to developmental regulation or effects. It is also reported that the bitter taste threshold increases with aging, especially in elderly people (Sergi 2017).

Human TRCs express 25 T2Rs, and each T2R contains 291 to 334 amino acids, share 23% to 86% sequence identity and respond to a wide range of compounds (Chandrashekar 2000, Conte 2002, Meyerhof 2010). These bitter receptors were first characterized in the year 2000 (Adler 2000). In this thesis, TAS2Rs is used whenever the genes coding the human bitter taste receptors are mentioned (according to the human genome organization gene nomenclature) and T2Rs is used whenever the human bitter taste receptor proteins are mentioned. All TAS2R genes are intronless and mapped to human chromosomes 12p and 7q, except for TAS2R1 which is mapped to chromosome 5p (Conte 2002). The T2R structure consists of a short extracellular N-terminus, seven transmembrane helices (TMs), three extracellular loops (ECLs), three intracellular loops (ICLs) and a short intracellular C-terminus. The structures of the TM regions are the most conserved among different T2Rs, while the rest of the sequence including ICLs, ECLs, N-

and C-termini is more variable. This feature corresponds well with the function of different fragments, since ECLs always form the ligand-binding pockets in T2Rs and ICLs regions are responsible for G-protein interaction. Until now the classification of T2Rs in GPCRs is still not clear, as T2Rs share low sequence similarity with other family members of GPCRs. Some described T2Rs as a separate family in the GPCR superfamily (Vroling 2011), while some classified them with frizzled/TAS2 sub-class of GPCRs (Fredriksson 2003).

Similar to all GPCRs, T2Rs are linked to heterotrimeric G proteins. The downstream G-protein signaling pathway for T2Rs were known prior to the discovery of T2Rs (Chandrashekar 2000). The taste-specific G-protein complex is made up of Gα-gustducin, β3 and γ13, and binds to GDP in its inactive state and GTP in active state (Wong 1996). In a T2R-expressing TRC in the oral cavity, the binding of bitter agonists to T2Rs lead to conformational changes of the receptors, which activate the G-protein complex. The Gα-gustducin then exchange the bound GDP for GTP, leading to the dissociation of β and γ subunits, which together activate the enzyme phospholipase C β2 (PLC β2). PLC β2 hydrolyzes inositol phospholipid (PIP_2) to 1,4,5-triphosphate (IP_3) and diacylglycerol (DAG) (Spielman 1994, Spielman 1996). The generated IP_3 molecules then bind to the IP_3 receptors located on the endoplasmic reticulum and this opens the calcium channel, causing transient increase in intracellular calcium levels (Akabas 1988). The increase in calcium level opens the transient receptor potential cation channel subfamily M member 5 (TRPM5), which induces cell membrane depolarization via increase in sodium ion influx. This in turn leads to release of neurotransmitter ATP, which activates the afferent nerves and transmit the taste information to the brain (Finger 2005).

(ii) Sweet and umami

Sweet taste is elicited by molecules such as soluble carbohydrates, artificial sweeteners. It helps humans in detecting food with high calories (Nelson 2001) (Behrens 2011). “Umami” is derived from a Japanese word “umai” which means savory. Umami taste is elicited by amino acids like glutamate, pyroglutamic acid, succinyl-Arg and succinyl-Glu, and is linked to protein intake (Zhao 2016). Umami taste modifiers are widely used in the food industry.

Three T1R receptors consisting of T1R1, T1R2 and T1R3 are responsible for sweet and umami sensing. The heterodimer formed by T1R2 and T1R3 mediate sweet taste, while the heterodimer formed by T1R1 and T1R3 mediate umami taste (Li 2002, Bachmanov and Beauchamp 2007). T1Rs belong to class C GPCR superfamily. They carry a signature of the Class C GPCR family, the large N-terminal domain termed as Venus flytrap (VFT) domain (Pin 2003). This VFT domain forms the orthosteric binding pocket to recognize ligands for T1Rs (Temussi 2009).

(iii) Salt and sour

Salt sensation is mainly induced by sodium, which can enter the cell by amiloride sensitive epithelial sodium channel (ENac) and induce the release of calcium, leading to salt sensation (Canessa 1994, Matsunami 2000). Sour is mainly caused by dietary acids, indicating rotten or fermented food. The transduction proteins responsible for sour are still not properly characterized. Previous studies suggested that organic acid permeates into TRCs and the intracellular H^+ can block a proton-sensitive channel (unidentified), which leads to membrane depolarization and exocytosis of neurotransmitters which transmit sour sensation (Chaudhari and Roper 2010) (Barlow 2015).

(iv) Other tastes

Studies also suggested there are other taste modalities like fat taste and carbon dioxide (CO_2) perception. Fat may be sensed by CD36, a plasma membrane glycoprotein (Mattes 2001, Laugerette 2005, Daoudi 2015) and CO_2 may be sensed by carbonic anhydrase 4 (Chandrashekar 2009). These are not considered as basic tastes, as yet.

.

1.5 T2R expression in extra-oral tissues

Over the last decade, many studies reported that in addition to the gustatory system, T2Rs were also expressed in various extraoral tissues, including gastrointestinal (GI) tract, airways (Shah 2009, Deshpande 2010, Tizzano 2010), vasculature (Upadhyaya 2014), heart (Foster 2013), testis (Li and Zhou 2012), thyroid (Clark 2015), immune system (Maurer 2015), skin (Wolfle 2015), brain (Singh 2011), breast cancer cells (Singh 2014), and bone marrow cells (Lund 2013) as recently reviewed by Shaik et al (Shaik 2016).

Intriguingly, the activation of T2Rs expressed in extraoral tissues leads to various physiological and pathophysiological cellular responses. For example, asthma is an airway disease characterized by airway obstruction and bronchospasm, and β_2-adrenergic receptor agonists are currently used to dilate airway smooth muscles. Recent study showed that activation of T2Rs expressed in airways smooth muscle cells leads to a bronchodilatory effect which was suggested to be three-fold greater than that caused by β_2-adrenergic receptor activation (Deshpande 2010), suggesting the potential anti-asthmatic role of T2Rs. T2Rs expressed in GI tract are able to sense hormones and nutritional contents inside the lumen and may help reject the ingestion of toxic substances (Wu 2002). The activation of T2R1 expressed on human pulmonary arterial smooth muscle cells (hPASMCs) leads to

vasoconstrictor responses (Upadhyaya 2014). It is also reported that T2Rs expressed in breast cancer cells are functional (Singh 2014). Other functions of T2Rs include detecting bacterial stimulant in upper airways (Tizzano 2010, Lee 2012), sensing nutrients in heart (Foster 2013), and acting as targets for tocolytics to prevent preterm birth (Zheng 2017). The activation of T2Rs may also lead to additional drug effects. Many pharmaceutical drugs including antibiotics are bitter in taste which means these are efficient bitter agonists. For these drugs, the extra-oral expression of T2Rs may be responsible for their side effects (Clark 2012).

1.6 Constitutive activity of T2Rs

Constitutive or spontaneous activity is the ability of the receptor to produce a downstream signal in the absence of an agonist. Until now, there are over 60 wild-type GPCRs from different species discovered to exhibit constitutive activity (Seifert and Wenzel-Seifert 2002). Some naturally occurring GPCR mutants, or non-synonymous single nucleotide polymorphisms (nsSNPs), also have high constitutive activity and they are predominantly disease-causing (Seifert and Wenzel-Seifert 2002). These mutants with high constitutive activity are called constitutively active mutants (CAMs). Since CAMs have high basal activity, they can be used to characterize inverse agonists.

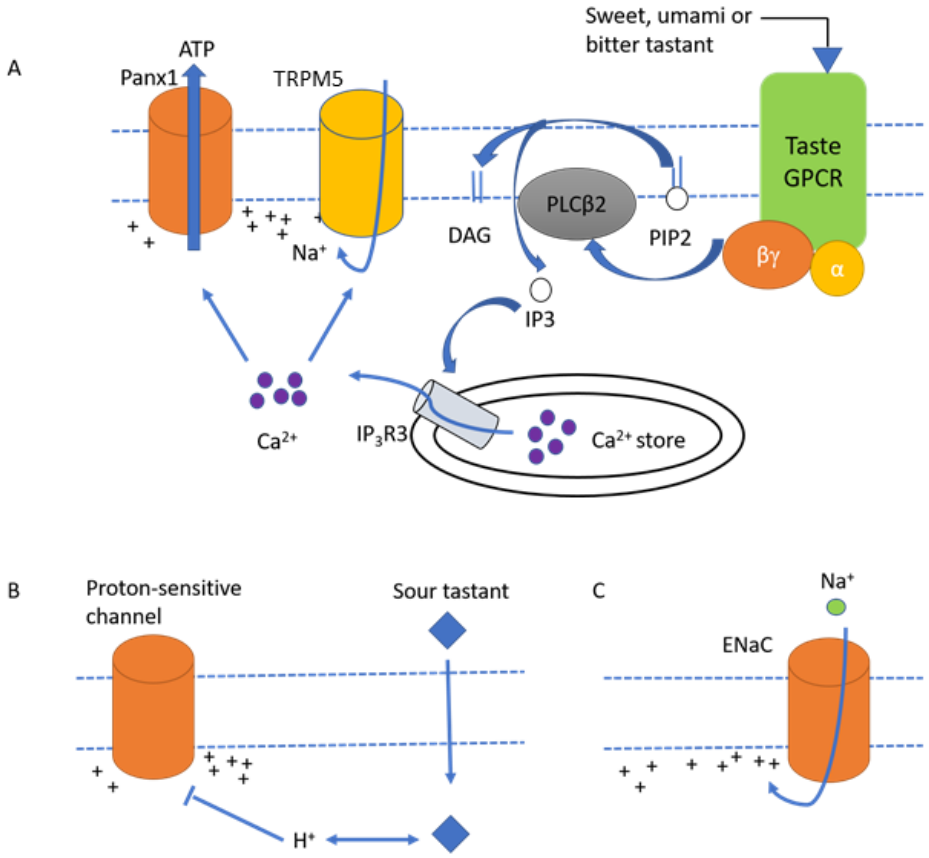

Figure 4 The signaling mechanisms of the five basic tastes. A. After activation by corresponding agonists, bitter, sweet or umami receptors change their conformations and activate PLC β2 signaling pathway, leading to intracellular calcium mobilization, membrane depolarization through TRPM5, and ultimately ATP release. **B.** Sour taste is elicited by acids, which penetrate into the cytoplasm. The intracellular H^+ blocks the proton-sensitive channel, leads to membrane depolarization and the release of synaptic vesicles. **C.** The taste of salt is evoked by Na^+ through ENac. In each of the above basic tastes, the intracellular mechanisms in the case of bitter or sweet or umami, and protein targets in the case of sour, are not clear yet.

None of the wild type T2Rs or T2R nsSNPs were reported to have constitutive activity. Based on an alanine scan mutagenesis of ICL3 in T2R4, the H214A mutant was found to display a 10-fold increase in constitutive activity over wild-type T2R4, (Pydi 2014). As this amino acid is conserved in 24 T2Rs, it was speculated that this histidine is crucial in stabilizing T2R structures, and mutating this histidine may lead to high constitutive activity in other T2Rs as well.

1.7 Classification of T2R ligands

Ligands which bind to GPCRs are classified into three predominant categories, agonists, antagonists and inverse agonists (Figure 5). An agonist is a ligand which binds to the receptor and leads to downstream signalling. Antagonists are neutral and they induce no response after binding to the receptor, however they can inhibit the function of other ligands (like agonists) in a competitive manner (Kenakin 2004). Inverse agonists also block the function of other ligands, but unlike antagonists, they bind to receptors and dislodge the bound G-proteins and thus decrease the basal activity of the receptors (Sato 2016). As CAMs have high basal activity, they can be used as pharmacological tools to identify new inverse agonists or distinguish between antagonists and inverse agonists.

In humans, 25 T2Rs have been identified thus far. T2Rs detect numerous structurally diverse ligands which includes phenols, hydroxyl azacycloalkanes, fatty acids, peptides, amino acids and their derivatives, amines, amides, N-heterocyclic compounds, ureas, thioureas, carbamides, metal ions, fatty acids, lactones, crown ethers, halogenated or acetylated sugars, secoiridoids, carbonyl compounds, glycosides, alkaloids, flavonoids,

terpenoids, steroids, and esters (Meyerhof 2010). Some receptors like T2R10 and T2R14 were reported to show broad ligand specificity, while some receptors like T2R3, T2R5 and T2R42 show very narrow ligand specificity with only a few known ligands (Wiener 2012). It is of great interest to study how these 25 receptors are able to recognize such a large number of ligands of different structures. A recent study on T2R16 suggested that in the ligand-binding pocket formed by the hydrophobic residues, some residues contribute to ligand specificity while some are responsible for the signal transduction of all ligands, thus the ligand-binding pocket can bind diverse ligands while still maintaining high specificity (Thomas 2017).

1.8 Computational methods for T2R study

Computational methods are requisite for T2R structural investigations, as there are no crystal structures elucidated for T2Rs. Combined with biological experiments, computational methods can provide new insights into T2R ligand binding and signaling mechanisms. By using homology model guided site-directed mutagenesis, Pydi et al elucidated T2R4 residues involved in the binding of agonist quinine (Pydi 2014). This study also identified two potent T2R4 blockers, γ-aminobutryic acid (GABA) and Nα,Nα-bis(carboxymethyl)-L-lysine (BCML) (Pydi 2014). By using a Molecular Mechanics/Coarse Grained method for structure predictions (Leguebe 2012), a previous study investigated the ligand pocket of phenylthiocarbamide (PTC) and propylthiouracil (PROP) to T2R38 which was confirmed by site-directed mutagenesis and calcium mobilization assays (Marchiori 2013).

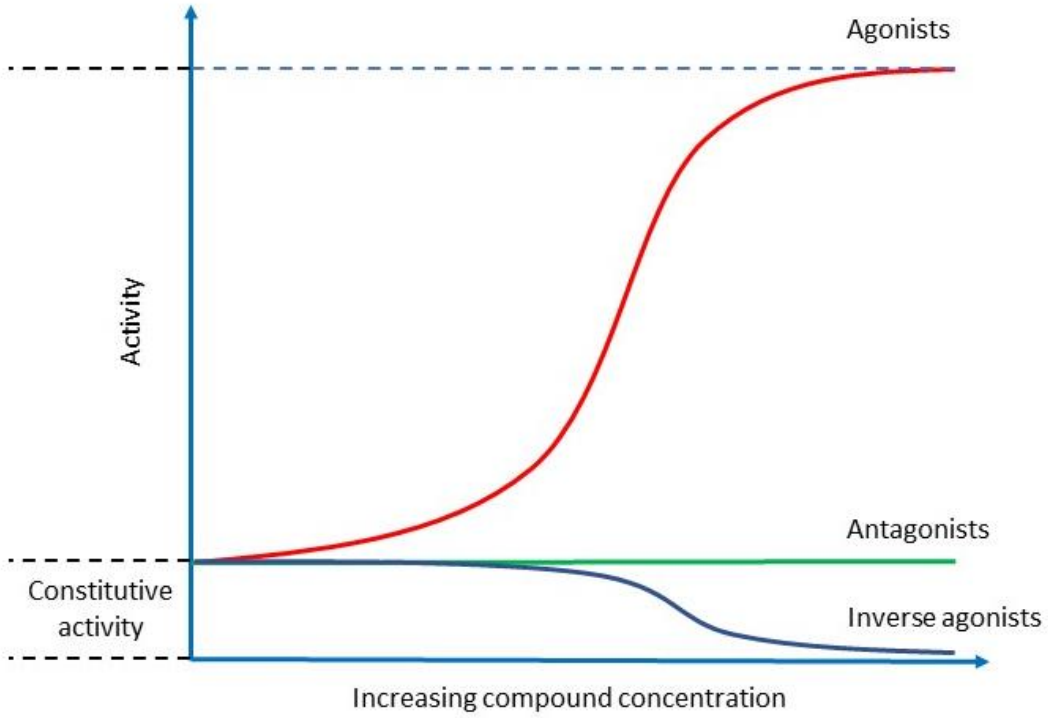

Figure 5 Schematic representation of the effects of agonists, antagonists and inverse agonists. Agonists activate the receptor and significantly increase the activity. Antagonists bind to receptor but produce no effect. Inverse agonists stabilize the receptor and supress the basal activity.

1.9 Peptides as T2R ligands

Recently small peptides generated from proteins (such as milk proteins, soybeans, fish etc.) through food processing, aging processes or enzymatic processes have become a popular research topic, due to their importance in food industry and their potential biological activities (Zhao 2016). Many of these peptides were reported to have angiotensin converting enzyme (ACE) inhibitory activity, which means they have the potential to reduce blood pressure (Liu 2017, Mirzapour 2017). *In vivo* studies have shown that ACE inhibitory peptides were able to reduce the blood pressure in spontaneous hypertensive rats, which are the most frequently used animal models for hypertension (Saito 1994, Nakamura 1995, Miguel 2005). A significant number of these peptides are also responsible for the bitterness in the fermented products and the protein hydrolysates (Maehashi and Huang 2009). Casein, a major constituent of cow's milk, produces the most bitter hydrolysates which is able to reduce deer browsing significantly (Kimball 2005). Soy protein products also present bitterness, which has received quite a lot attention because of their important functions in physiology, particularly in the prevention of chronic diseases related to aging (Wang and De Mejia 2005).

To improve the gustatory properties of protein foodstuffs, the structural features of bitter peptides have been widely studied (Maehashi and Huang 2009). Kim et al suggested that a peptide is more likely to be bitter with a bulky hydrophobic residue at the C-terminus and a bulky basic residue at the N-terminus (Kim and Li-Chan 2006). Proline is also a predominant contributor to bitterness as proline-containing peptides are more likely to bind to T2Rs (Zhao 2016). Notably, Zhao et al reviewed bitter taste peptides and found bitter

peptides and ACE-inhibiting peptides share similar structure features, and many bitter dipeptides exhibited ACE-inhibitory activity (Zhao 2016).

CHAPTER 2

RATIONALE, HYPOTHESIS AND OBJECTIVES

2.1 Rationale

In view of the emerging role of T2Rs in extraoral tissues, it is of significant biomedical importance to characterize T2Rs and identify efficient T2R ligands. As T2Rs are involved in various physiological and pathophysiological effects, they are promising drug targets for the treatment of diseases, such as asthma. A previous study hypothesized that all bitter drugs elicit off-target effects through extraorally expressed T2Rs (Clark 2012). This suggests the high potential for bitter blockers in curtailing some of the additional effects of bitter tasting drugs. Bitter blockers may also improve the palatability of bitter-tasting foods.

T2R7 is one of the bitter receptors with little information on its ligand specificity, amino acid residues involved in ligand binding, and mechanisms of receptor activation. Several ligands have been reported for T2R7 (Table 1), but no structure-function studies on T2R7, have been published. In this study, the discovery of new ligands and structure-function studies for human bitter taste receptor T2R7 was pursued.

2.2 Hypothesis

The bitter taste receptor T2R7 has broad ligand specificity and ligands bind to an orthosteric site on its extracellular side.

To address this hypothesis, two objectives were pursued.

2.3 Objectives

2.3.1 Specific objective 1

To identify and characterize potential T2R7 ligands from commercial and natural sources.

2.3.2 Specific objective 2

To characterize the ligand specificity of T2R7 by homology model guided site-directed mutagenesis of amino acids involved in ligand binding.

Table 1 T2R7 reported agonists

No.	Agonists	EC_{50} or Threshold values (μM)	Reference	Additional information
1	Strychnine	Not determined	(Sainz 2007)	Not confirmed by Meyerhof et al (Meyerhof 2010)
2	Quinacrine	Not determined	(Sainz 2007)	
3	Chloroquine	Not determined	(Sainz 2007)	Not comfirmed by Meyerhof et al (Meyerhof 2010)
4	Papaverine	10 (Threshold)	(Meyerhof 2010)	
5	Caffeine	300 (Threshold)	(Meyerhof 2010)	Activate mainly T2R43 and T2R46, not T2R7 (Suess 2016)
6	Quinine	10 (Threshold)	(Meyerhof 2010)	
7	Chlorpheniramine	10 (Threshold)	(Meyerhof 2010)	
8	Cromolyn	4500 ± 1600 (EC_{50})	(Meyerhof 2010)	
9	Diphenidol	10 (Threshold)	(Meyerhof 2010)	
10	H.g.-12	30 (Threshold)	(Le Neve 2010)	Poor solubility of H.g.-12 and its aglycon in buffer at concentrations > 250 μM limited the calculation of EC50.
11	Malvidin-3-glucoside	12.6 ± 0.7 (EC_{50}); 6.0 (Threshold)	(Soares 2013)	
12	Chloral hydrate	1460 (Threshold)	(Ji 2014)	

CHAPTER 3

MATERIALS AND METHODS

3.1 Materials

3.1.1 Cell lines and cell culture materials

All T2R7 studies were conducted using Human Embryonic Kidney (HEK293T) cell line which was purchased from ATCC (Cat # CRL-3216, Manassas, VA, USA). HEK293T cells or transfected HEK293T cells were cultured at 37°C with 5% carbon dioxide (CO_2) in Steri-cycle CO_2 incubator (Thermo Scientific, Canada). The cell-culture medium used is DMEM-F12 (Gibco, Life technologies, Carlsbad, CA, USA) supplemented with 10% FBS (Sigma, USA) heat-inactivated at 55°C for 40 min, and 1% Penicillin-Streptomycin (Gibco, Life technologies).

Tissue culture material including 10 cm dishes, 6-well, 12-well and 24-well plates were purchased from Corning Life Sciences (Lowell, MA, USA). Centrifuge tubes 15 ml and 50 ml and tips for pipettes were purchased from VWR International (Mississauga, ON, Canada). Adjustable volume pipettes were purchased from Gilson (Guelph, ON, Canada). Sterile disposable plastic pipettes were purchased from Greiner (Mississauga, ON, Canada).

Trypsin-EDTA (0.5%, 10X) for cell dissociation was purchased from Gibco Life technologies, cell-culture grade dimethyl sulfoxide (DMSO) for cell freezing was from Sigma Aldrich (Oakville, ON, Canada).

3.1.2 Chemical and bitter compounds

Bitter compounds (±) - Chlorpheniramine maleate salt (Cat # C3025), caffeine (Cat # C0750), chloroquine diphosphate salt (Cat # C-6628), cromolyn sodium salt (Cat # C0399), denatonium benzoate (Cat # D5765), dextromethorphan hydrobromide (Cat # D9684), diphenhydramine hydrochloride (Cat # D3630), quinine hydrochloride (Cat # Q1125), sodium thiocyanate (Cat # 251410), strychnine hydrochloride (Cat # S8753), thiamine hydrochloride (Cat # T1270), azithromycin (Cat # PHR1088), ciprofloxacin HCl (Cat # PHR1044), levofloxacin hemihydrate (Cat # PHR1697), tobramycin sulfate salt (Cat # T1783) and (-)-erythromycin hydrate (Cat # 856193), C4-AHL (Cat # 09945), 3-oxo-C8-AHL (Cat # 10940), 3-oxo-C12-AHL (Cat # O9139) and 2-heptyl-e-hydroxy-4-quinolone (Cat # 94398) were purchased from Sigma Aldrich. Diphenidol hydrochloride (Cat # D486940) was purchased from TRC (Toronto, ON, Canada), and 2-nonyl-3-hydroxy-4-Quinolone (Cat # 9002699) was purchased from Cayman.

3.1.3 Calcium assay reagents

Calcium sensitive dye Fluo-4 NW kit was purchased from Life technologies (Carlsbad, CA USA), 96-well black-walled microtiter plates with clear bottom were purchased from International BD Biosciences (Mississauga, ON, Canada). Clear 96-well V-bottom compound plates were purchased from Greiner. Calcium assay reading machine Microplate reader Flexstation 3 and black tips used for the calcium assay were purchased from Molecular devices (Sunnyvale, CA, USA).

3.1.4 Plasmid DNA extraction kits and transfection reagents

QISprep Spin miniprep Kit and QIAGEN plasmid Maxi Kit were purchased from QIAGEN (Toronto, ON, Canada). RedGel Nucleic Acid stain was from Biotium (Burlington, ON, Canada). pcDNA 3.1 was purchased from Life technologies (Burlington, ON, Canada). Restriction digestion enzymes Not1 and Kpn1 were from New England Biolabs (Ipswich, MA, USA). Lipofectamine 2000 was purchased from Invitrogen, T2R7 and mutant plasmids were synthesized commercially (GenScript Inc., MA, USA). Nano drop 2000 (Thermo Scientific) was used to measure the concentration of plasmid DNA.

3.1.5 Flow cytometry reagents

Allophycocyanin (APC) anti-DYKDDDDK Tag antibody (Clone L5) was purchased from BioLegend (San Diego, CA, USA). Bovine Serum Albumin (BSA) was purchased from VWR Life Science. FACS (fluorescence-activated cell sorting) tubes (5 ml polystyrene round-bottom tube, 12 × 75 mm style) were purchased from Falcon, Corning.

3.2 Preparation of buffers and media

3.2.1 Buffers

Agarose loading buffer (10ml):

150 mM Tris (pH7.6)	3.3 ml
Bromophenol blue	25 mg
Glycerol	6 ml

Add Milli-Q water to 10 ml.

Phosphate Buffered Saline (PBS) 10X (1 L):

KCl	1 g
KH_2PO_4	1.2 g
NaCl	40 g
Na_2HPO_4	5.7 g

Dissolve in Milli-Q water and add water to 1 litre. The pH was adjusted to 6.8.

Phosphate Buffered Saline (PBS) 1X (1 L):

PBS 10X	100 ml
Water	900 ml

Adjust pH to 7.4.

Tris Acetate-EDTA (TAE) buffer 10X (1 L):

Glacial acetic acid (17.4 M)	11.4 ml
Tris	48.4 g
0.5 M Na_2EDTA (pH 8.0)	20 ml

Add water to make to 1 litre.

TAE buffer 1X (1 L):

TAE 10X	100 ml
Water	900 ml

FACs buffer:

0.5% BSA dissolved in 1X PBS.

3.2.2 Media

DMEM/F12 basal (1 L):

Dulbecco's Modified Eagle Medium Nutrient Mixture F12 (Ham) (1:1) powder 15.6 g (gibco, life technologies), dissolved in 1 L Milli-Q water and supplemented with 1.2 g/L $NaHCO_3$. The pH was adjusted to 7.25.

DMEM/F12 + + (500 ml):

DMEM/F12 medium	445 ml
Heat inactivated FBS	50 ml
Pen Strep	5 ml

Luria-Bertani (LB) media (1 L):

Tryptone	10 g
Yeast extract	5 g
Sodium chloride	10 g

Dissolve in 1 litre Milli-Q water.

LB-agar plates (100 µg/ml ampicillin) preparation:

In a 1 L flask, 7.5 g of agar was added into 500 ml LB media and the suspension was autoclaved. The medium was allowed to cool down to about 55°C at room temperature. One percent or 500 µl of 100 mg/ml ampicillin was added to 500 ml of the medium to make the final ampicillin concentration 100 µg/ml. Then the agar-containing medium was poured into the sterile petri dishes at 20-25 ml/plate. The agar-medium was solidified at room temperature and stored at 4°C.

3.3 Methods

3.3.1 Construction of human TAS2R7 wild-type and mutant gene-containing plasmids

Human TAS2R7 gene (NCBI Accession ID # NC_000012.12) with an N-terminal FLAG sequence was codon-optimized for expression in mammalian cells (GenScript Inc., MA, USA). The TAS2R7-FLAG gene consist of 1007 bp, includes a sequence coding octa-peptide FLAG tag DYKDDDDK after the ATG start codon, and restriction enzymes sites for KpnI at the 5' end and NotI at the 3' end. This gene is then cloned into the KpnI-NotI site of pcDNA 3.1/Hygro (+) expression vector. The nucleotide and amino acid sequences of wild-type TAS2R7 and mutants are shown in Figure 6.

3.3.2 Transformation of competent *E. coli* (DH5α) with wild-type and mutant TAS2R7 plasmids

To amplify the plasmids, TAS2R7 wild-type and mutant plasmids were transformed into *E. coli* (DH5α). *E. coli* competent cell stock stored at -80°C was thawed on ice, from which 50 µl was taken and mixed with 0.4 µg of plasmid DNA in a 1.5 ml Eppendorf tube. The *E. coli*-DNA mixture was kept on ice for 30 min, then placed at 42°C for 40s, followed by on ice for 2 min. Then 1 ml LB media was added to the *E. coli*-DNA mixture and further incubated in an orbital shaker in 37°C for 1 h with intense shaking at 240 rpm. After this step, 50 µl of the mixture was spread on LB-agar plate (100 µg/ml ampicillin). The plate is then placed at 37°C overnight to allow the formation of colonies.

3.3.3 Preparation of glycerol stocks

Individual colonies from the LB-agar plate were picked and each colony was incubated in 5 ml LB media (100 µg/ml ampicillin) separately in the orbital shaker (37°C, 240 rpm) and left to grow overnight (16 h). From the overnight culture 0.5 ml was added to 0.5 ml of 50% glycerol in a 1.5 ml Eppendorf tube. The stocks were immediately transferred into -80°C freezer. Whenever bacterial culture is needed for plasmid extraction, the *E. coli* cells were revived from these stocks.

3.3.4 Extraction of plasmids from *E. coli*

To obtain plasmids, *E. coli* glycerol stocks were inoculated in 5 ml LB-ampicillin medium using autoclaved sticks and left in the orbital shaker (37°C, 240 rpm) for 16 h. Then the plasmid DNA was extracted from the overnight culture using QIAprep Spin kit (to obtain 10-20 µg DNA) or QIAGEN plasmid Maxi kit (to obtain about 500 µg DNA) following instructions provided by the manufacturer.

3.3.5 Plasmid restriction digestion

To verify the size of the inserted DNA fragments in the plasmids, restriction digestion was performed as follows. Plasmid DNA 1 µg, 1 µl EcoRI buffer (NEB), 1µl 10 X BSA, 1 µl NotI (10 units), 1 µl KpnI (10 units) were mixed together and the volume was made up to 10 µl by adding Milli-Q water. The samples were incubated at 37°C for 2 h, and then mixed with 1 µl 10X loading dye to stop the reaction.

3.3.6 Agarose gel electrophoresis

Agarose gel (1%) was prepared by dispersing 0.5 g agarose into 50 ml 1X TAE and dissolved by heating in a microwave for about 80 s. The melted agarose solution was cooled to about 55°C and then 1.5 µl RedSafe nucleic acid staining solution (iNtRON Biotechnology, Korea) was added to allow the visualization of DNA under ultraviolet (UV) light. The agarose solution was then poured into gel tray and the comb was inserted to generate the loading wells. The agarose gel was allowed to solidify, and the gel was placed in a Bio-Rad Mini Sub Cell electrophoresis gel box filled with 1X TAE. DNA samples in 10X loading dye were added to the wells. 1 kb DNA Ladder (New England Biolabs) was used to estimate molecular weight of DNA bands. The electrophoresis was run at 100 V for 50 min or till the front band had migrated two thirds of the gel. The results were visualized under UV light using FluorChem FC2 (ProteinSimple, Santa Clara, CA, USA).


KpnI
Kozak
Flag tag
ggtaccgaattcgccaccatggactacaaggacgatgacgataaagcagataaggtgcag
G T E F A T M D Y K D D D D K A D K V Q
accacactgctgttcctggccgtgggagagttttctgtcggcattctggggaacgccttc
T T L L F L A V G E F S V G I L G N A F
atcggcctggtgaattgcatggactgggtcaagaaaaggaaaatcgctagcattgatctg
I G L V N C M D W V K K R K I A S I D L
atcctgacctcactggcaattagccgcatctgcctgctgtgcgtgattctgctggactgt
I L T S L A I S R I C L L C V I L L D C
D65A
(gcg)
D65E
(gaa)
tttatcctggtgctgtaccccgatgtctatgctaccgggaaggaaatgaggatcattgac
F I L V L Y P D V Y A T G K E M R I I D
D86A
(gcg)
D86E
(gaa)
ttcttttggactctgaccaaccacctgagcatctggttcgcaacatgcctgtccatctac
F F W T L T N H L S I W F A T C L S I Y
W89A
(gcg)
W89H
(cat)
tatttctttaagatcggcaatttctttcatccactgtttctgtggatgaagtggcgaatt
Y F F K I G N F F H P L F L W M K W R I
gacagagtgatcagctggatcctgctggggtgcgtggtgctgtccgtcttcatctctctg
D R V I S W I L L G C V V L S V F I S L
cccgcaactgagaacctgaatgccgatttcagattttgcgtgaaggccaaaaggaagaca
P A T E N L N A D F R F C V K A K R K T
aacctgacttggtcctgtcgggtgaacaagacccagcacgcatctacaaagctgttcctg
N L T W S C R V N K T Q H A S T K L F L
N167A T169A
(gcg) (gcg)
N167Q T169S
(cag) (agc)
S181A
(gcg)
S181T
(acc)
W170A
(gcg)
W170H
(cat)
aacctggccacactgctgccttttgcgtgtgcctgatgagtttctttctgctgattctg
N L A T L L P F C V C L M S F F L L I L
tcactgcggagacacatcaggcgcatgcagctgtctgccactggatgccgcgatccaagt
S L R R H I R R M Q L S A T G C R D P S
H211A
(gcc)
accgaggctcatgtgcgagccctgaaggctgtcattagcttcctgctgctgtttatcgct
T E A H V R A L K A V I S F L L L F I A
tactatctgtccttcctgattgcaacaagctcctactttatgcccgagactgaactggcc
Y Y L S F L I A T S S Y F M P E T E L A
T255A
(gcg)
T255S
(agc)

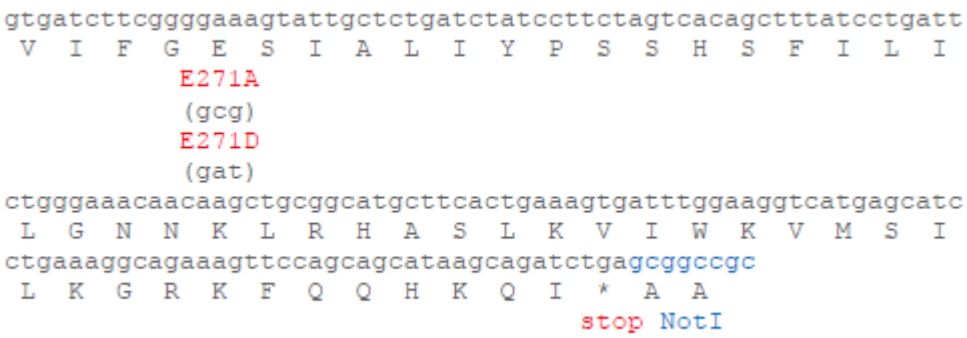

Figure 6 DNA (nucleotide) and amino acid sequences of codon-optimized T2R7 and T2R7 mutants. The KpnI and NotI restriction sites flank the receptor sequence and are shown in blue. The start codon is shown in yellow and the Kozak sequence GCCACCATGG is shown in bold. The FLAG-tag sequence is shown in red. The T2R7 amino acid changes are shown in red and the corresponding codon sequence in black parentheses.

3.3.7 Transfection of HEK293T cells

HEK293T cells were used to express T2R7 wild-type (WT) or mutant receptors. HEK293T cells are a variant of HEK293 cells that stably express the large-T antigen, which promotes DNA replication. The procedure to generate HEK293T stable cell lines expressing a GPCR of interest has been described in detail elsewhere (Chakraborty 2015). Briefly, HEK293T cells were transiently transfected with T2R7 wild type- or mutant-containing plasmids using lipofectamine 2000 (3 µg: 3 µl, DNA: lipofectamine), and transfected cells were sparsely subcultured in 10 cm dish under hygromycin selection (150 µg/ml) to generate stable cell clones. The expression of the receptor in different clones was analyzed using flow cytometry and the functionality was analyzed by calcium mobilization assay.

3.3.8 Flow cytometry

The cellular expression of the WT or mutant receptors was measured by flow cytometry. For stable cell lines, HEK293T cells were used as control, and for T2R7 (WT or mutant) transiently-transfected cells, HEK293T cells transiently-transfected with empty pcDNA were used as control. Before assay, cells were plated in 6-well tissue culture plate and allowed to grow overnight, and then cells were lifted and 5×10^5 viable cells for each group (experimental or control cells) were collected in a 15 ml centrifuge tube, centrifuged for 3.5 min at 350 g, washed 3 times using cold FACs buffer and incubated with APC anti-DYKDDDDK antibody (1: 500 diluted in FACs buffer) for 1 h on ice. After incubation, cells were again washed 3 times, resuspended in 300 µl FACs buffer, transferred into FACs tubes and APC fluorescence measured by BD FACS Canto analyzer. FlowJo 7.6 software

program was used to analyze the results and calculate the mean fluorescence intensity (MFI).

3.3.9 Calcium assay

Fluo4-NW Calcium assay kit (Invitrogen) was used to measure the increase in intracellular calcium as mentioned in 3.1.3. HEK293T transfected or nontransfected cells were seeded into 96-well black walled plates with 70,000 viable cells per well. Cells in the black walled plates were incubated in cell culture incubator overnight, then the media was removed and the dye solution was added. Cells were incubated at 37°C for 35 min and at room temperature for 30 min after the addition of dye. The 96-well V-bottom compound plate loaded with different compounds was prepared. During the assay, predetermined amounts of compound solutions were transferred from compound plate to the assay plate by the automated pipette system in Flex station 3. The results were read by Flexstation 3 following excitation at 494 nm and emission at 525 nm.

3.3.10 T2R7 Molecular modeling

The T2R7 3D structure was built using I-TASSER (Iterative Threading ASSEmbly Refinement) server. T2R7 amino acid sequence (shown in Figure 6) was uploaded to I-TASSER server. I-TASSER generated several T2R7 templates from the PDB library based on sequence identity and multiple-threading approach LOMETS (Local Meta-Threading-Server). The structural domains from the identified protein templates were reassembled together to make the best homology or threading structure (based on identity). After the protein model was made, based on the protein structural quality the server reported five

T2R7 models. The best model was selected and minimized using PRIME module in Schrodinger software (11.0, 2017) until the minimum energy score was achieved. The quality of the model was checked using Procheck and Ramachandran plot (Laskowski 1996).

3.3.11 Ligand docking to T2R7 in Schrodinger

Before docking with the ligands, the T2R7 model from 3.3.10 was prepared using the Protein Preparation Wizard to get an all-atom structure with appropriate bond orders and formal charges. A grid area was generated around the extracellular site of the receptor (x = 75 Å, y = 53 Å, z = 70 Å) for ligand docking.

Four bitter compounds including quinine, diphenidol, dextromethorphan (DXM), and diphenhydramine (DXM) were docked to T2R7 model. The 2D chemical structures of the ligands were obtained from PubChem database and uploaded to Schrodinger, The structure of these ligands were optimized using Ligprep module. The optimized ligands were docked into T2R7 protein structure using Glide (SP & XP) module. This module searches for favorable interactions between one or more ligand molecules and the T2R7 model. Final scoring was then carried out on the ligand poses using *GlideScore* scoring function.

CHAPTER 4

RESULTS

4.1 T2R7 stable cell line generation

4.1.1 T2R7 plasmid manipulation

Wild-type (WT) and mutant T2R7 plasmids were transformed into *E. coli*, grown in 5 ml LB media, then extracted by plasmid MiniPrep (Qiagen) and verified using restriction digestion (Figure 7). The recombinant plasmids were digested by restriction enzymes Not1 and Kpn1. The empty pcDNA 3.1 with and without restriction enzyme digest were used as negative and internal control, respectively. T2R9 DNA plasmids (characterized previously in the lab) were used as positive control. The size of the empty pcDNA 3.1 is 5.4 kb. For the negative and internal controls, the bands for the inserted genes were absent, as expected. In the positive control group and T2R7 group, the bands of the inserted genes were shown around 1 kb. T2R7 genes are 1007 base-pair long, which is consistent with the results obtained. T2R7 mutant H211A was also verified along with WT-T2R7 (Figure 7).

4.1.2 Characterization of T2R7 stable cell lines

The T2R7 in HEK293T stable cell line was generated following the protocol described in 3.3.7. The surface expression of T2R7 receptor was determined by flow cytometry (Figure 8). The T2R7 WT and mutant plasmid constructs built in this study had a FLAG-tag attached to the N-terminus, which allowed the cell surface receptors to be detected by anti-FLAG antibody. The calcium assay shows that the T2R7 stable cell line

responds to a greater degree to both quinine (1 mM) and diphenidol (0.5 mM), which are two known T2R7 agonists (Figure 8) as compared to non-transfected HEK293T cells.

4.2 T2R7 ligand screening

In order to characterize the ligands T2R7 interacts with, twenty compounds (or compound mixtures) including eight reported T2R7 agonists were tested. The molecules (unreported as T2R7 ligands) tested included five bitter compounds, five antibiotics and two bacterial quorum sensing molecule mixtures. T2R7 stable cell line was treated with these compounds and cytoplasmic calcium levels were measured. In each case, two concentrations of the compounds were selected based on either the reported EC_{50} values, threshold values for T2R7 or other T2Rs, or the solubility of the compounds (Table 2).

4.2.1 Responses of T2R7 to eight reported agonists

The eight reported agonists including strychnine, chloroquine, caffeine, quinine, chlorpheniramine, cromolyn, diphenidol and malvidin-3-glucoside were tested for their ability to activate the T2R7 receptor. Among these eight compounds, strychnine and chloroquine were reported to be T2R7 agonists by Sainz et al using an reconstitution system (not cell based) (Sainz 2007), however these were not confirmed by Meyerhof et al in cell based assays (Meyerhof 2010). Our results showed that the T2R7 receptor responded to strychnine, caffeine, quinine, chlorpheniramine and diphenidol at both concentrations, however no response was observed for chloroquine, cromolyn or malvidin-3-glucoside (Figure 9).

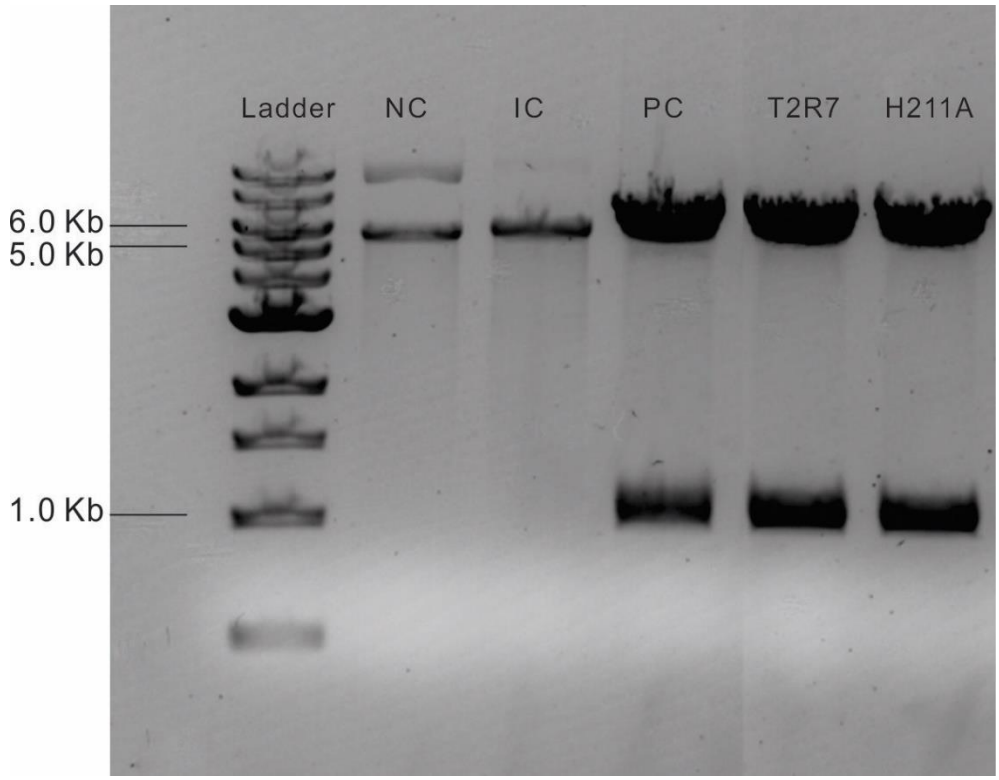

Figure 7 Agarose gel electrophoresis (1%) of the restriction enzyme digest of recombinant plasmids. A representative agarose gel (1%) with the DNA ladder in the first lane is shown. For the negative control (NC), the vector (alone) pcDNA3.1 was added with no restriction enzymes, for the internal control (IC), pcDNA3.1 digested with restriction enzymes NotI and KpnI, and for the positive control (PC) group, pcDNA3.1-T2R9 recombinant was used. As shown in the figure, T2R7 wild-type and mutant plasmids digested with NotI-KpnI run as two fragments, the smaller fragment is the inserted gene which is about 1 Kb long, and the cut vector runs around 6 Kb.

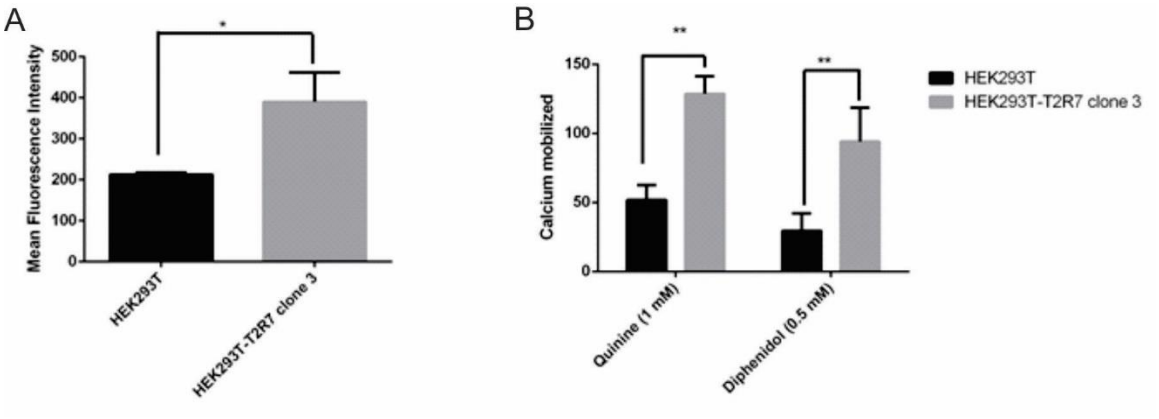

Figure 8 T2R7 stable cell line characterization. A. Flow cytometry was used to analyze the expression of T2R7 receptor on the cell surface. HEK293T cells and the selected clone HEK293T-T2R7-clone3 are represented on x-axis, and mean fluorescence intensity (MFI) on y-axis. Surface staining was performed using APC conjugated anti-FLAG antibody. HEK293T cells were used as a negative control. MFI was calculated using FlowJo software. The data represents two independent experiments performed in duplicate. Results were analyzed by student's t-test (*$p<0.05$). **B.** Bar graph showing cytoplasmic calcium levels (ΔRFU) in HEK293T (control) cells and T2R7 stable cell line (clone 3) to 1 mM quinine and 500 µM diphenidol treatment. T2R7 clone 3 showed significant higher response to 1 mM quinine and 500 µM diphenidol compared to HEK293T control cells. The data represents three independent experiments performed in triplicate. Results were analyzed by student's t-test (**$p<0.01$).

4.2.2 Responses of T2R7 to common bitter compounds

The five new, previously unreported, bitter compounds tested on T2R7 were denatonium benzoate, dextromethorphan, diphenhydramine, sodium thiocyanate and thiamine hydrochloride. All of these compounds activate multiple T2Rs except dihenhydramine which is reported to activate T2R14 only (Wiener 2012). Among the five common bitter compounds, T2R7 responded to dextromethorphan at 1 mM and 0.5 mM, and diphenhydramine hydrochloride at 2 mM and 1 mM (Figure 10). Thiamine hydrochloride activated T2R7 at 6 mM, but showed completely no activation at 3 mM (Figure 10).

4.2.3 Responses of T2R7 to antibiotics and quorum sensing molecules

Most antibiotics are bitter in taste, which makes them potential T2R agonists. Five prescription antibiotics, frequently used to treat airway bacterial infection were tested for their ability to activate T2R7 receptors. The antibiotics levofloxacin, ciprofloxacin, tobramycin, azithromycin and erythromycin that were tested on control and T2R7 receptor transfected cells. Among these five antibiotics, tobramycin and erythromycin showed a modest activation on T2R7 as determined by changes in intracellular calcium levels (Figure 11).

Quorum sensing molecules are autoinducers through which bacteria communicate with each other to coordinate gene expression and regulate multicellular behaviour at a population level (Fuqua 1994). These autoinducers are able to mimic human hormones and signal to human cells as well (Hughes and Sperandio 2008). Whether T2R7 responds to these quorum sensing molecules remains to be elucidated. Two mixtures of the main quorum

sensing molecules secreted by the opportunistic airway pathogen *Pseudomonas aeruginosa* were applied to the T2R7 stably transfected cell line. These include Acyl-homoserine lactones (AHLs) consisting of N-(3-oxododecanoyl)–AHL (3-oxo-C12-AHL), N-(3-Oxooctanoyl)-L-(3-oxo-C8-AHL), and N-butyryl-AHL (C4-AHL) at 50 µM or 100 µM, and 2-Alkyl-4(1H)-quinolones (AHQs), 2-nonyl-4-hydroxy-quinoline (NHQ) and 2-heptyl-4-quinolone (HHQ) at 25 µM or 50 µM each. The concentration of the individual quorum sensing molecules in the mixture was based on solubility. In the assay conditions, it was the maximum concentrations that could be tested. Results showed that none of the quorum sensing molecules activated T2R7 (Figure 11).

4.3 Dose dependent characterization of T2R7 transfected cells stimulated with quinine, diphenidol, dextromethorphan and diphenhydramine

To determine the Half-Maximal Effective Concentrations (EC_{50}) of quinine, diphenidol, dextromethorphan (DXM) and diphenhydramine (DPH) for T2R7 stably transfected cells, concentration-dependent activation was examined and EC_{50} values were determined by nonlinear regression analysis using PRISM software version 6.01 (GraphPad Software Inc., San Diego, CA). The responses of control cells (non-transfected HEK293T cells) were subtracted. The EC_{50} values for quinine, diphenidol, DXM and DPH are 983 ± 257 µM, 675 ± 186 µM, 518 ± 19 µM and 634 ± 81 µM, respectively (Figure 12).

Table 2 Compounds used for T2R7 ligand screening.

No.	Compound	Conc.	No.	Compound	Conc.
1	Strychnine	2 mM, 1 mM	**11**	Sodium thiocyanate	3 mM, 1.5 mM
2	Chloroquine	2 mM, 1 mM	**12**	Thiamine hydrochloride	6 mM, 3 mM
3	Caffeine	5 mM, 2.5 mM	**13**	Diphenhydramine hydrochloride	2 mM, 1 mM
4	Quinine	1 mM, 0.5 mM	**14**	Levofloxacin hemihydrate	500 μM, 100 μM
5	Chlorpheniramine	2 mM, 1 mM	**15**	Ciprofloxacin hydrochloride	500 μM, 100 μM
6	Cromolyn	3 mM, 1.5 mM	**16**	Tobramycin sulfate salt	500 μM, 100 μM
7	Diphenidol	1 mM, 0.5 mM	**17**	Azithromycin	500 μM, 100 μM
8	Malvidin-3-glucoside	50 μM, 10 μM	**18**	(-)-erythromycin hydrate	500 μM, 100 μM
9	Denatonium benzoate	1 mM, 0.5 mM	**19**	AHL mixture (C4-AHL, 3-oxo-C8-AHL and 3-oxo-C12-AHL)	100 μM, 50 μM
10	Dextromethorphan hydrobromide	1 mM, 0.5 mM	**20**	HHQ (2-heptyl-e-hydroxy-4-quinolone) and NHQ (2-nanoyl-3-hydroxy-4-quinolone) mixture	50 μM, 25 μM

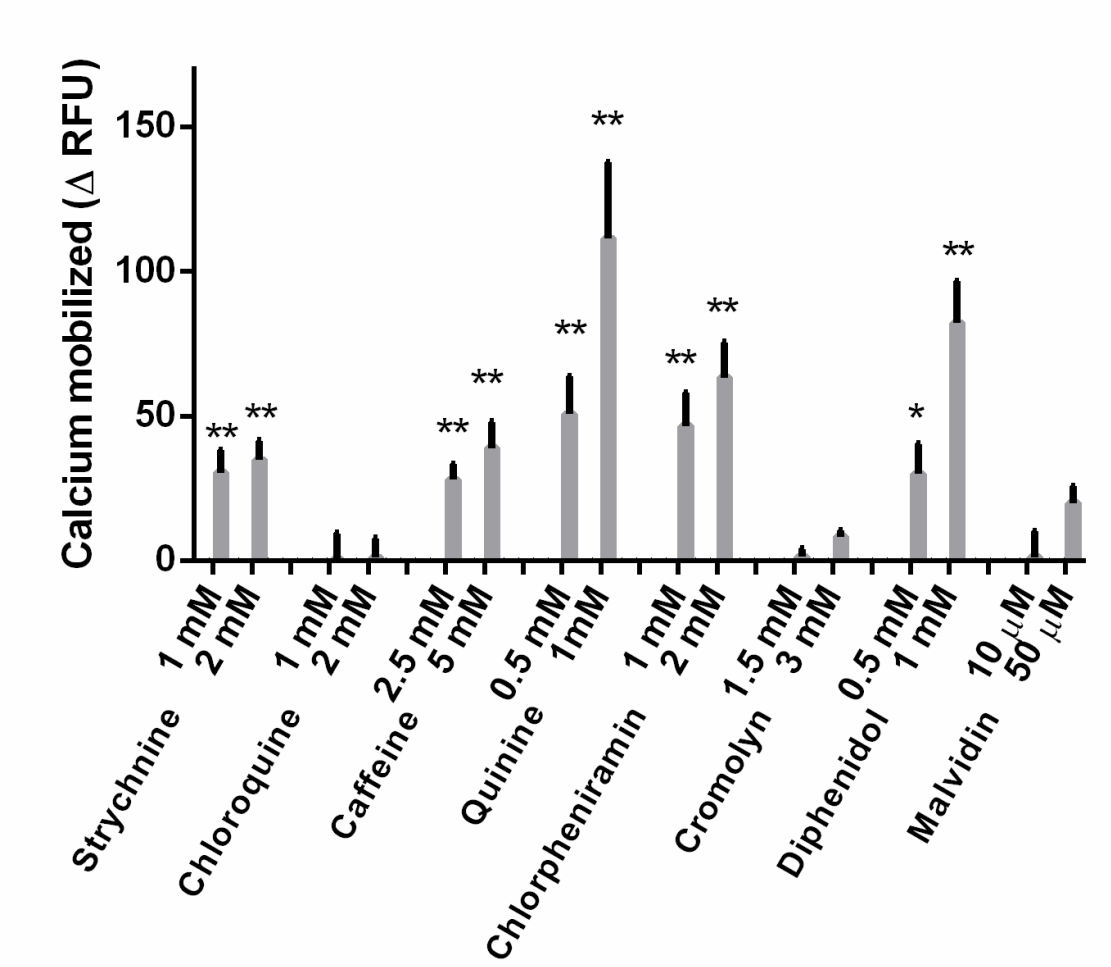

Figure 9 Calcium responses of T2R7 to eight previously reported agonists. Statistical significance of response differences in control cells and T2R7 stable cells was determined by student's t-test. Of the eight compounds, T2R7 showed significant responses to both concentrations of strychnine, caffeine, quinine, chlorpheniramin and diphenidol compared to control cells. The results after subtracting the baseline responses of control HEK293T cells to different compounds were shown. No response was observed with 2 mM or 1 mM chloroquine, 3 mM or 1.5 mM cromolyn, and 50 μM or 10 μM Malvidin-3-glucoside (*$p<0.05$, **$p<0.01$).

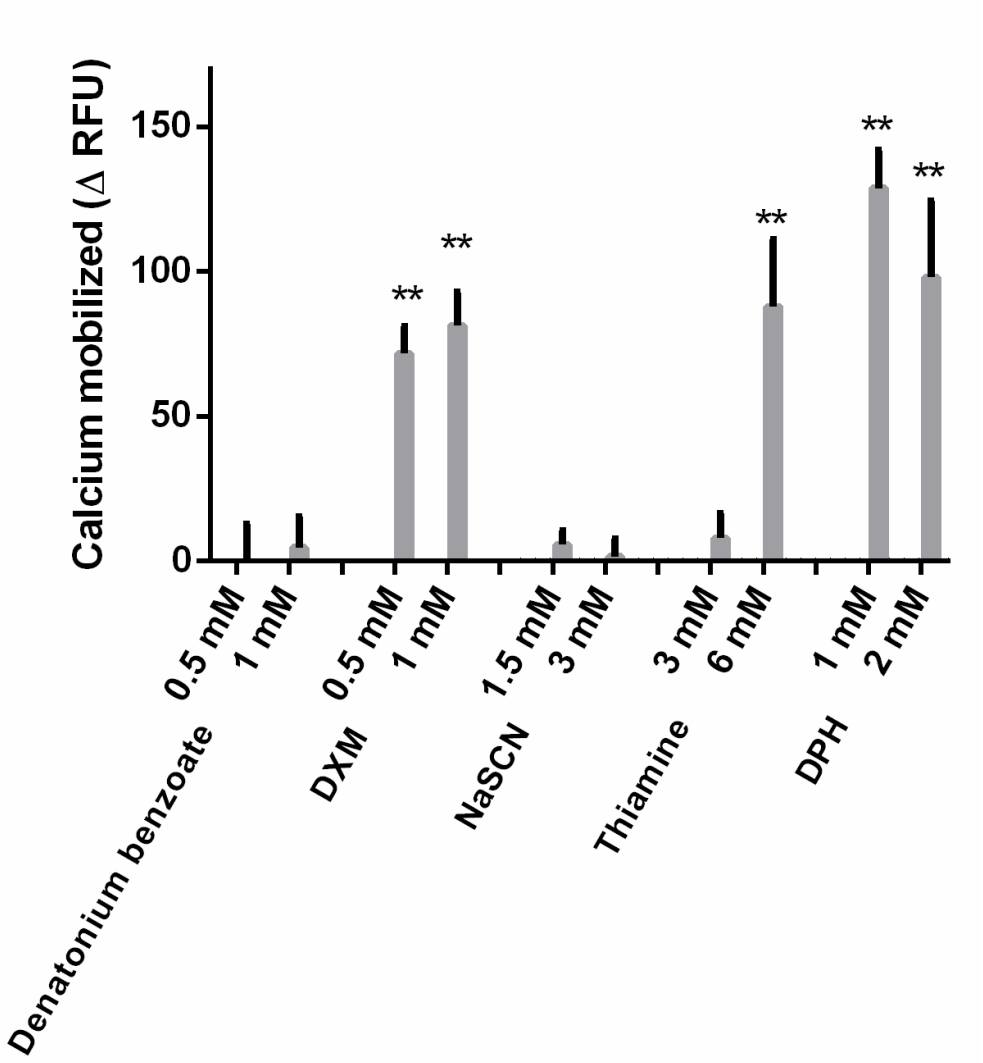

Figure 10 Calcium responses of T2R7 to new (unreported) bitter compounds. Statistical significance of response differences was determined by student's t-test. Among the five bitter compounds, T2R7 showed significant responses to dextromethorphan and diphenhydramine hydrochloride at both concentrations, and thiamine hydrochloride at 6 mM compared to control cells (*$p<0.05$, **$p<0.01$). The results after subtracting the baseline responses of control HEK293T cells to different compounds were shown.

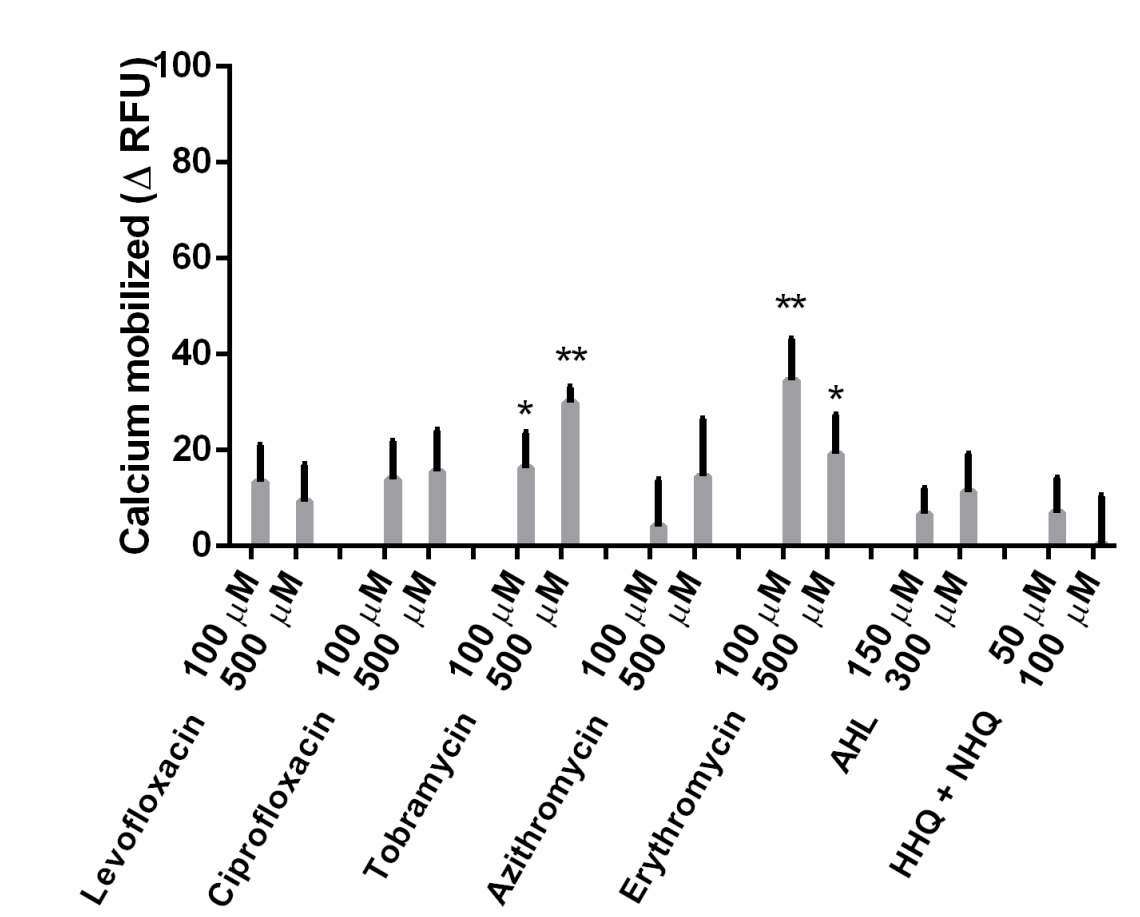

Figure 11 Calcium responses of T2R7 to antibiotics and quorum sensing molecules. Results was analyzed by student's t-test. The antibiotics were tested at two concentrations, 500 µM and 100 µM. The acyl homoserine lactones (AHLs) mixture contains C4-AHL, 3-oxo-C8-AHL and 3-oxo-C12-AHL, each at 100 µM and 50 µM. Mixture of the other quorum sensing molecules contains HHQ (2-heptyl-e-hydroxy-4-quinolone) and NHQ (2-nanoyl-3-hydroxy-4-quinolone) at 25 µM and 50 µM each. The results after subtracting the baseline responses of control HEK293T cells to different compounds were shown. The results showed that T2R7 responded to tobramycin and erythromycin at both concentrations compared with control cells (*$p<0.05$, **$p<0.01$).

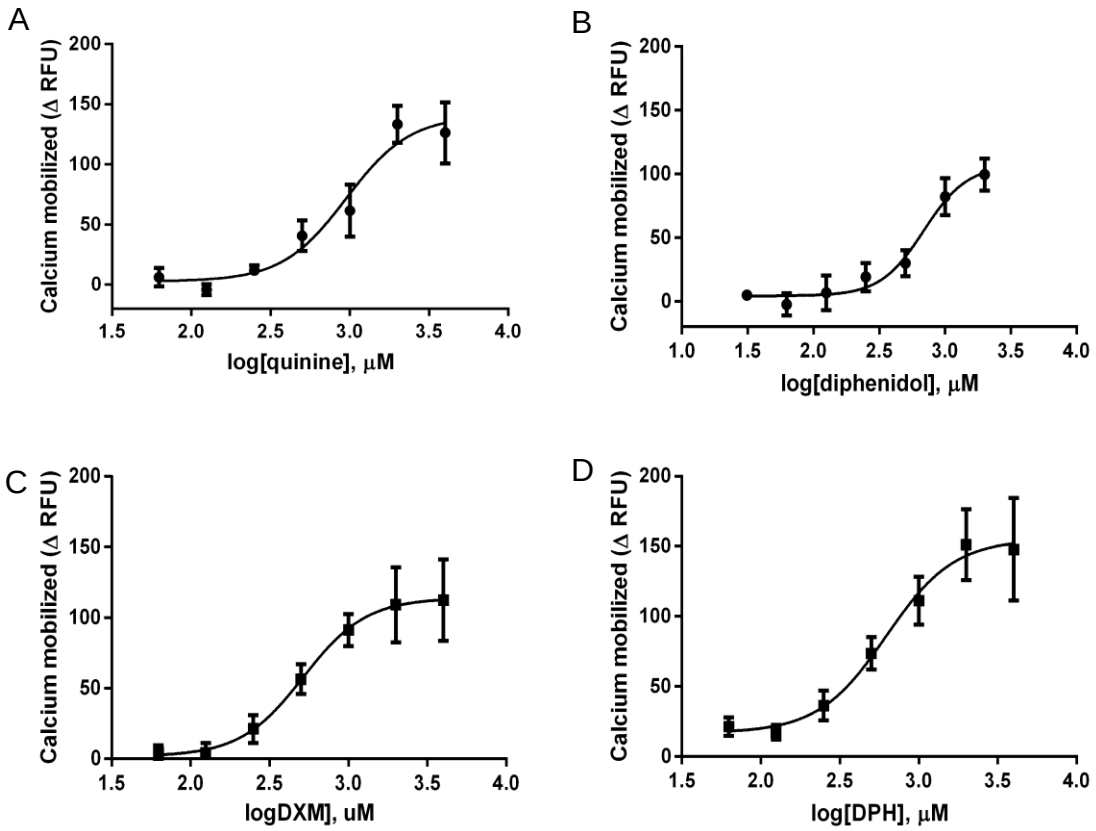

Figure 12 Concentration-dependent calcium response of T2R7 stable cells treated with quinine, diphenidol, dextromethorphan (DXM) and diphenhydramine (DPH). T2R7 expressing HEK293T stable cells were treated with different concentrations of (**A**) quinine ranging from 0.0625 to 4 mM, (**B**) diphenidol from 0.03125 to 2 mM, (**C**) DXM from 0.0625 to 4 mM, and (**D)** DPH from 0.0625 to 4 mM, respectively. Relative fluorescence unit (ΔRFU) was calculated by subtracting the baseline response of control HEK293T cells and EC_{50} values were determined. The EC50 values for quinine, diphenidol, DXM and DPH are 983 ± 257 μM, 675 ± 186 μM, 518 ± 19 μM and 634 ± 81 μM, respectively. The data represented is from five independent assays performed in duplicate or triplicate. EC_{50} values were determined by nonlinear regression analysis using PRISM software version 6.01 (GraphPad Software Inc., San Diego, CA).

4.4 Identify potential T2R7 ligands from beef protein hydrolysates

Previous studies have explored the relationship between peptides and bitterness (Maehashi and Huang 2009, Rauh 2014). Many peptides isolated from protein hydrolysates or fermented foods have been identified as having a bitter taste. It was previously reported that T2R1 receptor could be activated by dipeptides and tripeptides (Maehashi 2008, Upadhyaya 2010). Based on these previous studies, I analyzed beef protein hydrolysates to determine whether these hydrolysates may contain ligands for the T2R7 receptor.

4.4.1 Primary fractions from beef protein hydrolysates tested on T2R7

Beef proteins were hydrolyzed by alkalase and chymotrypsin, and then each hydrolysate was separated into four fractions by RP-HPLC (A1 to A4 fractions from alcalase hydrolysate, and C1 to C4 fractions from chymotrypsin hydrolysate, work done by Dr. Rotimi Aluko's laboratory). These fractions were separated mostly based on hydrophobic character as described previously (Girgih 2013). These initial fractions were then tested on cells stably transfected with T2R7 using the intracellular calcium assay. Results showed that A3 and C2 (5 mg/ml) activated T2R7, however the activation is significantly less than 1 mM quinine ($p < 0.05$). When T2R7 stable cells were treated with 1 mM quinine mixed with 5 mg/ml fractions, the fractions significantly blocked the quinine induced T2R7 activity (Figure 13).

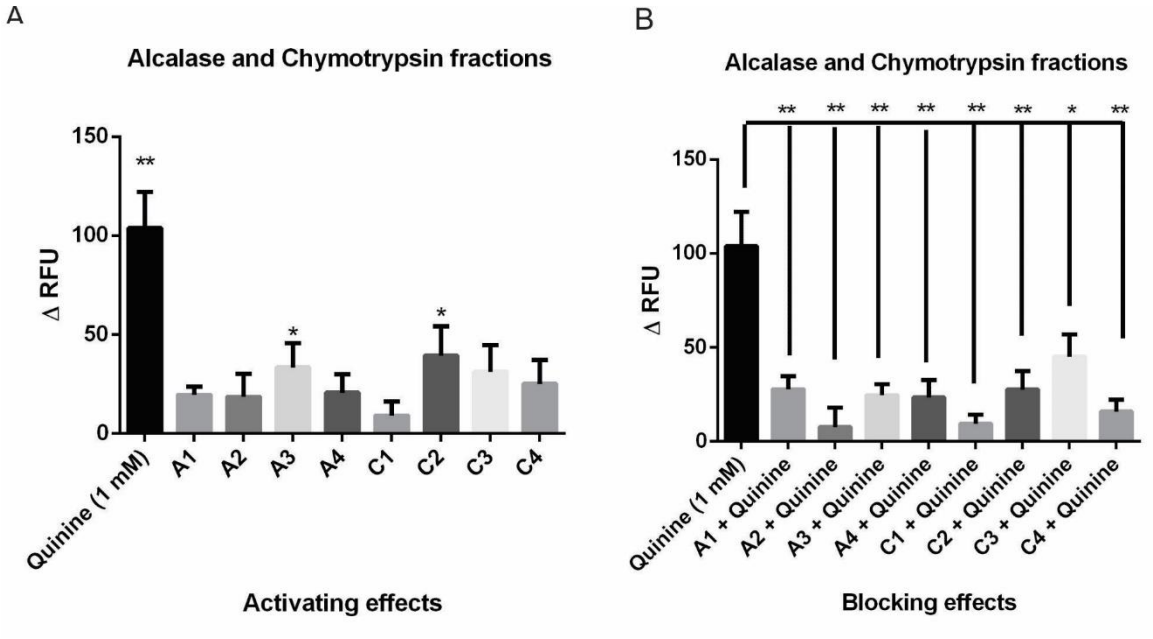

Figure 13 Functional response of T2R7 stable cells to alcalase and chymotrypsin treated beef protein hydrolysates. The baseline responses of control cells were deducted. **A.** The activating effects of eight fractions on T2R7. T2R7 stable cells were treated with quinine (1 mM) and all eight fractions (5 mg/ml), respectively. A3 and C2 showed a relatively low activation comparing to 1 mM quinine. **B.** Blocking effects of eight fractions on quinine mediated T2R7 activation. T2R7 stable cells were treated with 1 mM quinine mixed with fractions (5 mg/ml) to check if these fractions act as blockers. All eight fractions blocked the activity of quinine on T2R7 (*$p<0.05$, **$p<0.01$).

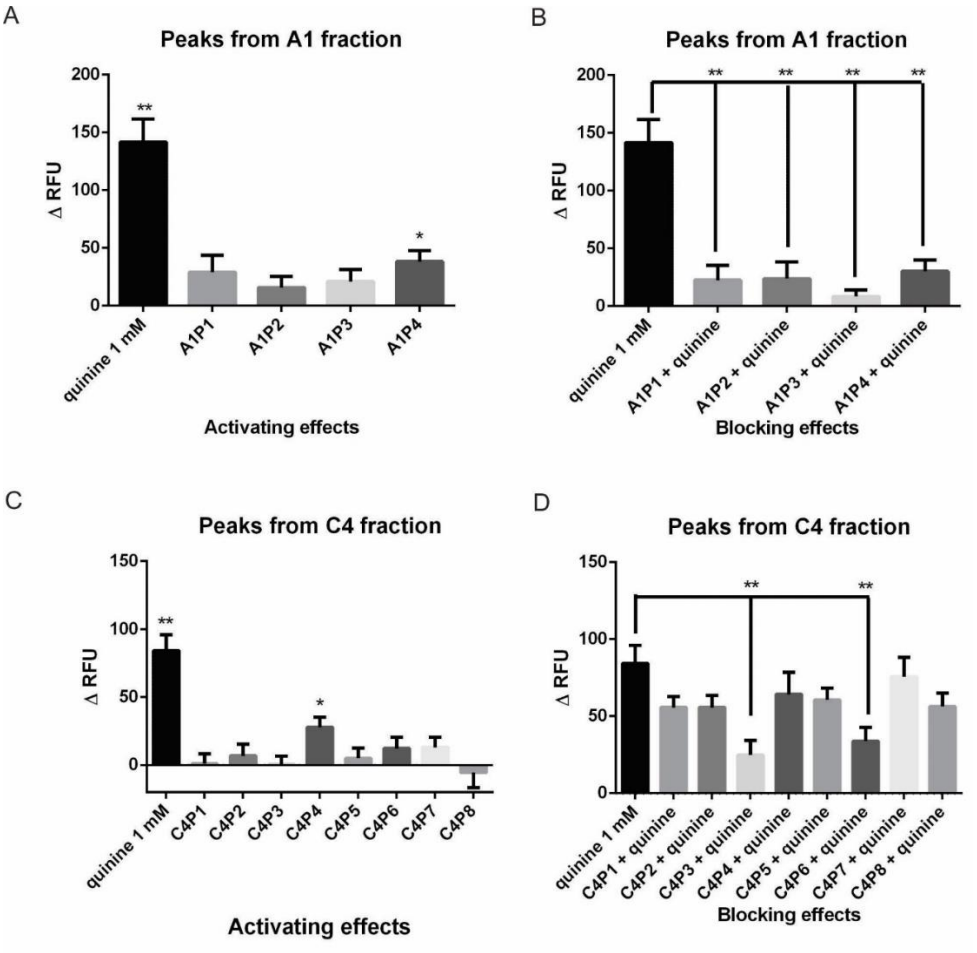

Figure 14 Functional responses of T2R7 stable cells to different beef protein hydrolysate fractions collected from A1 and C4. A. Effects of A1 fractions on T2R7. T2R7 stable cells were treated with quinine (1 mM) and A1 fractions (1 mg/ml). A1P4 caused a lower activation compared to 1 mM quinine. **B.** Blocking effects of A1 fractions on T2R7. T2R7 stable cells were treated with quinine mixed with different A1 fractions, all four fractions blocked the function of quinine on T2R7. The response of T2R7 cells to quinine was quenched to ~30 ΔRFU (from ~140 ΔRFU). **C.** Effects of C4 fractions as T2R7 agonists. C4P4 was showed a modest ability to activate T2R7. **D.** Blocking effects of C4 fractions on T2R7. Compared with the response caused by quinine alone, C4P3 and C4P6 significantly blocked the function of quinine (*$p<0.05$, **$p<0.01$).

4.4.2 Further purification of the primary fractions

Among the eight fractions, A1 and C4 were selected for further purification on RP-HPLC, and different peaks from these two fractions were collected separately. Four peaks were collected from A1 fraction (A1P1 to A1P4) and eight peaks were collected from C4 (C1P1 to C1P8) by Dr. Aluko's laboratory. To elucidate the main components of the peak fractions that could act as T2R7 blockers in 4.4.1, all these RP-HPLC fractions were again tested on cells stably transfected with T2R7. Like primary fractions, none of these RP-HPLC fractions caused any high activation of T2R7 as quinine. All four RP-HPLC fractions from A1 fraction blocked quinine induced T2R7 activity, while only two RP-HPLC fractions from C4, C4P3 and C4P6 showed blocking effect (Figure 14).

4.5 Characterization of constitutive activity of H211A mutant in T2R7

A previous study reported that the H214A mutant in T2R4 has a 10-fold increase in constitutive activity over wild-type T2R4, and this amino acid, histidine, is conserved in 24 human T2Rs (Pydi 2014). It was proposed that this conserved histidine, which is H211A in T2R7, might play a critical role in stabilizing the inactive structure of the T2Rs. To elucidate whether the H211 also plays a critical role in stabilizing the inactive T2R7 structure, characterization of H211A mutant was pursued. To characterize the constitutive activity of the H211A mutant in T2R7, the effect of cell surface receptor density on basal calcium mobilization was examined for WT-T2R7 and H211A. HEK293T cells were transfected with three different amounts of DNA (DNA: Lipofectamine ratios were 0.75 µg : 1.5 µl, 1.5 µg : 3 µl and 3 µg: 6 µl), then the basal activity of the transfected cells was

determined by calcium assay and the surface receptor expression was determined by flow cytometry. As the amount of DNA and Lipofectamine increased, the cell surface receptor density as well as the basal activity of the transfected cells, increased. If a mutant is constitutively active it will show a higher slope of expression vs. basal activity than WT receptor. The slope of the H211 mutant did not show any statistically significant difference from wild type T2R7 (Figure 15). This suggests that H211 in T2R7 is not a constitutively active mutant (Figure 15).

4.6 T2R7 molecular model building and ligand docking

A 3D structure of T2R7 was built by I-TASSER server. The model is shown in Figure 16. T2R7 receptor consists of 318 amino acids. The four T2R7 agonists, quinine, diphenidol, dextromethorphan and diphenhydramine that were pharmacologically characterized in section 4.3 were docked to the T2R7 model. Ligands were docked to the 3D molecular structure as described in methods. The docking results suggested that the binding pocket of T2R7 is located on the extracellular side. The ligand binding pocket in T2R7 model is predominantly formed by the extracellular part of the TM regions and regions of the extracellular loops. Based on the docking results, nine amino acid residues interacting with the ligands were selected for mutagenesis. These nine residues are D65, D86, W89, N167, T169, W170, S181, T255 and E271.

4.7 Mutagenesis guided by the T2R7 molecular model

To elucidate amino acids involved in ligand binding in T2R7, molecular model guided mutagenesis was performed. Two types of mutations were made for each selected

amino acid, replacement with a simple amino acid such as alanine or with a conservative substitution. Alanine mutagenesis were performed with the expectation that alanine will have minimum effect on receptor structure and ligand binding. Conservative substitutions like aspartate to glutamate, and tryptophan to histidine were expected to have similar function as the wild type receptor. The following 18 mutations were commercially synthesized (Genescript Inc, USA), D65A, D65E, D86A, D86E, W89A, W89H, N167A, N167Q, T169A, T169S W170A, W170H, S181A, S181T, T255A, T255S, E271A, E271D. Figure 17 shows 2D representation of T2R7 with the amino acids mutated highlighted.

4.8 Characterization of the expression of WT-T2R7 and T2R7 mutants

To investigate whether the mutations affect T2R7 receptor folding and trafficking, flow cytometry was used to determine the cell surface expression. As the WT-T2R7 and mutants express the FLAG epitope tag at the N-terminus, flow cytometry was used on non-permeabilized but transiently transfected HEK293T cells to determine cell surface expression of the receptor and mutants. The mean fluorescence intensity (MFI) of control cells (pcDNA 3.1 transfected HEK293T cells) was deducted from the MFI of WT-T2R7 and mutants (Figure 18). No statistically significant difference in protein expression was observed between the WT-T2R7 and mutants (Figure 18).

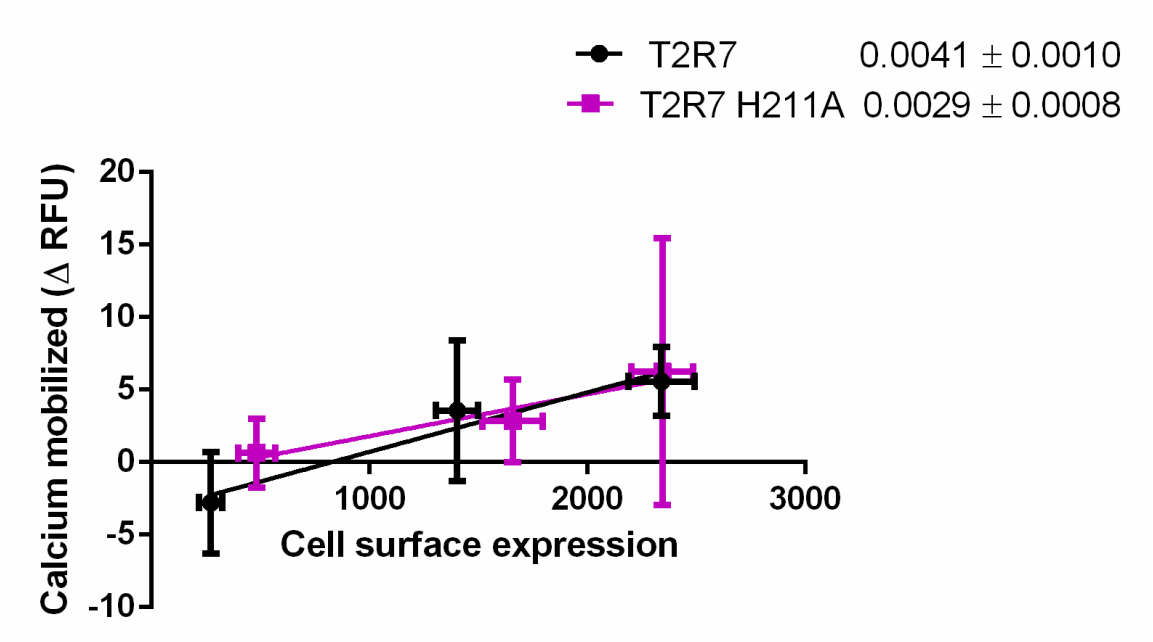

Figure 15 Pharmacological characterization of the basal activity of WT-T2R7 and H211A mutant. Cell surface expression was shown on x-axis and calcium mobilization on y-axis. The slope values were shown above next to the receptor names. In this assay, H211A mutant did not display higher constitutive activity compared to WT-T2R7 receptor.

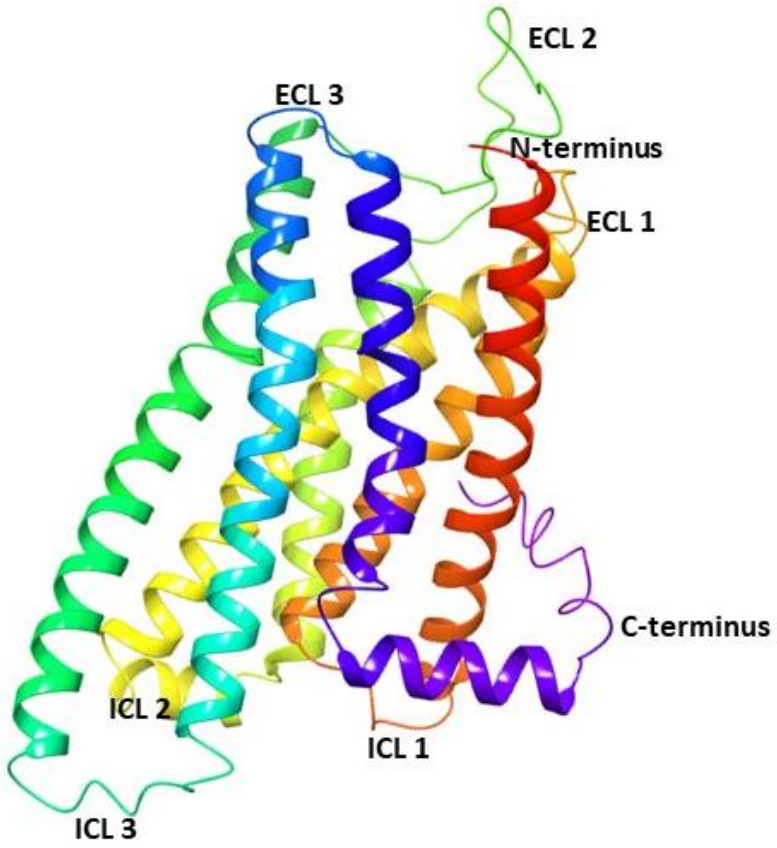

Figure 16 Molecular model of T2R7. T2R7 model is made up of seven transmembrane (TM) helices, a short extracellular N-terminus, three extracellular loops (ECLs), three intracellular loops (ICLs) and an intracellular C-terminus. The T2R7 model is built as described in methods and the image is prepared using Schrodinger software.

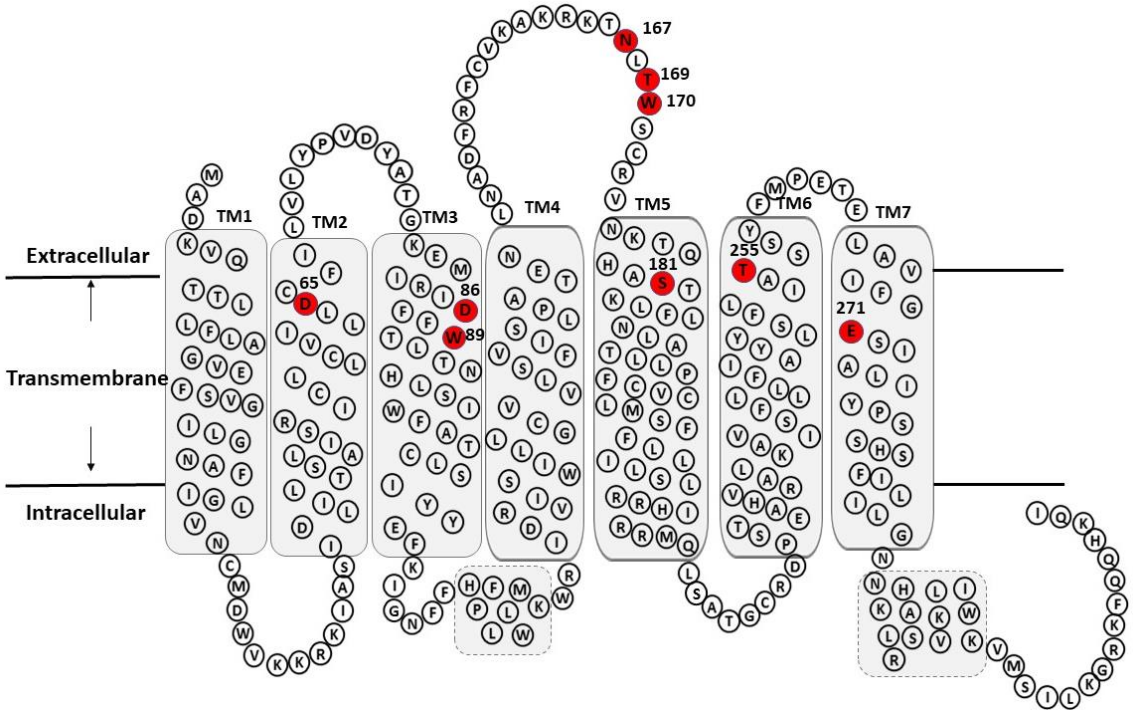

Figure 17 Two-dimensional representation of T2R7 amino acid sequence. The FLAG octapeptide sequence at the N-terminus after methionine start codon is not shown in the 2D structure for simplicity. T2R7 amino acid sequence contains 318 residues, which forms a short N-terminus, seven transmembrane (TM) helices, three extracellular loops (ECLs), three intracellular loops (ICLs), and an intracellular C-terminus. ICL3 starts from S207 to L234 according to TMHMM and HMMTOP server, which is different from I-TASSER prediction. The mutated amino acid residues that are predicted to be involved in ligand binding are highlighted in red. Three of these residues are present in ECL-2, and the rest on the extracellular side of the TM helices 2, 3, 5, 6 and 7.

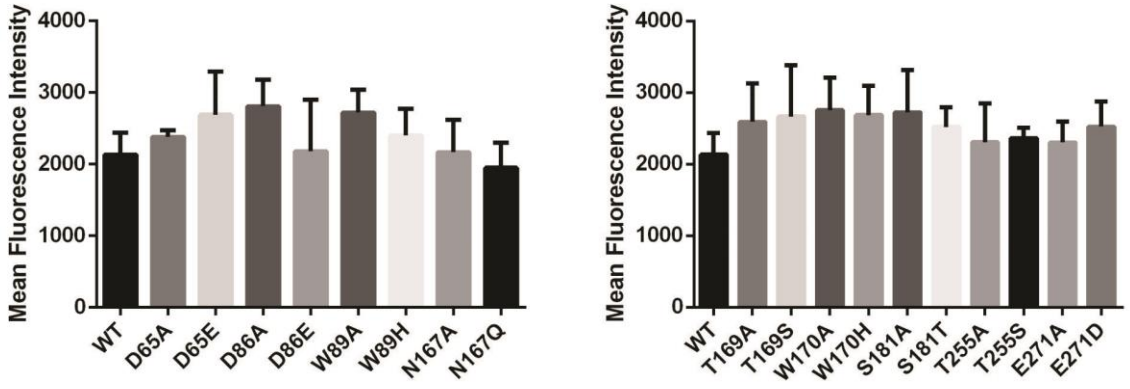

Figure 18 Cell surface expression of WT-T2R7 and mutants. Samples are shown on X-axis and cell surface expression (MFI) on Y-axis. The MFI value from mock-transfected cells (pcDNA 3.1 transfected cells) of 115.4 ± 29 MFI was subtracted from T2R7-WT and mutant values. Dunnett's multiple comparison test was performed to analyze the results. No statistically significant difference in receptor expression was observed between T2R7-WT and mutants. The results are from three independent experiments in duplicate.

4.9 Functional characterization of T2R7 mutants

To investigate the structural features in T2R7 that might contribute to the observed differences in ligand specificities (Figure 12), pharmacological characterization of the amino acid replacements lining the putative ligand binding pocket was pursued. Based on the ligand screening, quinine and dextromethorphan were selected as the ligands to functionally characterize the mutants. The rationale is based on their pharmacological profile; quinine has relatively high EC_{50} for T2R7, while dextromethorphan has the lowest EC_{50} for T2R7 among the four ligands (Figure 12).

The mutants were treated with different concentrations of quinine and dextromethorphan ranging from 0.0625 to 4 mM, and the calcium response (mobilized) was determined. The concentration-dependent curves of the WT-T2R7 and mutants to quinine and dextromethorphan are shown in Figures 19 and 20, respectively. Analysis of the quinine binding suggests mutations of five amino acids D65, W89, T169, T255 and E271 showed a significant left shift in the curves suggesting increased ligand affinity and/or hypersensitive receptor (Figure 19). Interestingly, this is independent of the type of mutation (alanine or a conservative substitution). Upon mutation of the residues D86, W170 and S181, significant loss of affinity towards quinine was observed. In striking contrast, for dextromethorphan only N167Q and T169 mutants showed increased affinity as suggested by a left shift of the response curves (Figure 20). Mutation of the rest of the amino acids showed a significant right shift in the response curves, suggesting decreased affinity or loss of dextromethorphan binding.

The pharmacological characterization of WT-T2R7 and the mutants upon treatment with quinine and dextromethorphan are summarized in Tables 3 and 4, respectively. There is no significant difference in expression of the mutants compared to WT-T2R7 thus eliminating the possibility of misfolded proteins influencing ligand binding. The "EC_{50} mutant / EC_{50} WT-T2R7" ratio gives a quantitative estimate of the gain or loss of ligand binding. A value significantly less than one (<1) implies increased ligand affinity and a value significantly more than one (>1) suggests decreased ligand affinity. Interestingly, the mutants D65E, W89A and E271A displayed significant hyperactive responses (E_{max}) to both quinine and dextromethorphan (Tables 3 and 4). However, T255S and T255A mutants showed contrasting hyperactive responses to quinine (E_{max} 118 ±18 ΔRFU for T255S) and dextromethorphan (E_{max} 110 ±16 ΔRFU for T255S), respectively.

4.10 Molecular model of T2R7 binding pocket

Analysis of molecular models of T2R7 bound to quinine and dextromethorphan (DXM) suggests that only D86 present on TM3 makes a direct contact with both ligands (Figure 21). In case of DXM, the negatively charged D86 makes a salt bridge with the N1 of DXM (Figure 21). This might explain the more significant effects of the D86 mutants on DXM binding (Table 4). The other interactions observed are predominantly hydrophobic, such as with Pi-Pi stacking interactions of DXM with W89 on TM3. Based on the molecular model it can be concluded that the residues in ECL2, specifically N167, T169 and W170 are in close proximity to the bound ligands and might influence ligand binding. However, given the limitations of these molecular models with predicting the movement of ECL2, precise information could not be obtained about the role of the amino acids in ECL2. The residue N167 is conserved 100% in T2Rs, and was suggested to be N-

glycosylated in T2R16 (Reichling 2008). It was shown in T2R16 that glycosylation is important for receptor maturation but not for its function. In this study, no difference in cell surface expression was observed for N167 mutants compared to WT-T2R7 (Figure 18). Interestingly, the N167 mutants showed slightly altered ligand affinities with N167Q showing increased affinity for dextromethorphan (Figures 19 and 20). These effects are probably due to the position of N167 in the crucial part of ECL2 influencing ligand binding rather than the possibility of N-glycosylation of N167 having an effect, though it cannot be ruled out as the glycosylation status of N167 was not analyzed in this study. Molecular simulation studies might give more insights into the role of these residues in T2R7 activation and ligand binding.

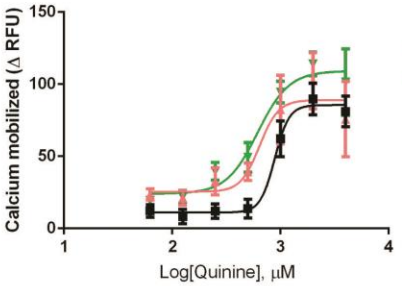
Calcium mobilized (Δ RFU)
Log[Quinine], μM
WT
D65A
D65E

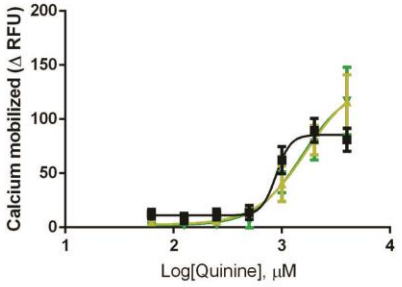
Calcium mobilized (Δ RFU)
Log[Quinine], μM
WT
D86A
D86E

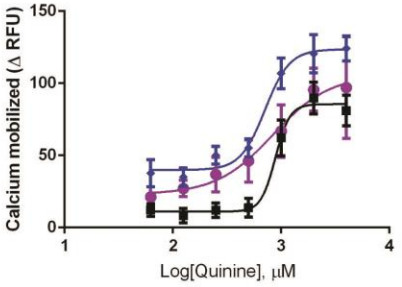
Calcium mobilized (Δ RFU)
Log[Quinine], μM
WT
W89A
W89H

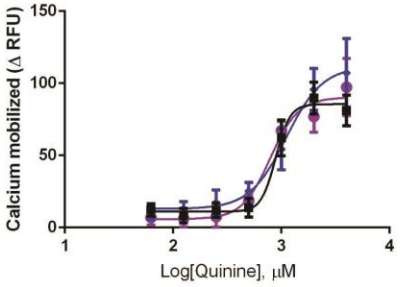
Calcium mobilized (Δ RFU)
Log[Quinine], μM
WT
N167A
N167Q

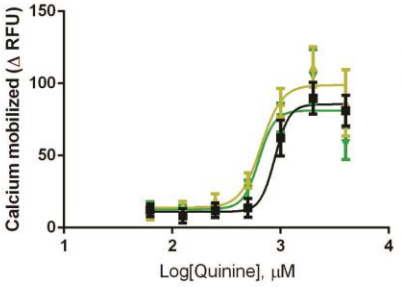
Calcium mobilized (Δ RFU)
Log[Quinine], μM
WT
T169A
T169S

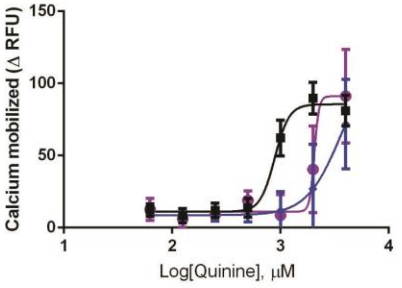
Calcium mobilized (Δ RFU)
Log[Quinine], μM
WT
W170A
W170H

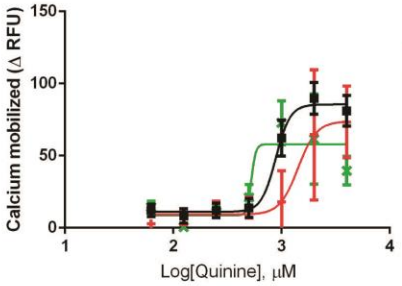
Calcium mobilized (Δ RFU)
Log[Quinine], μM
WT
S181A
S181T

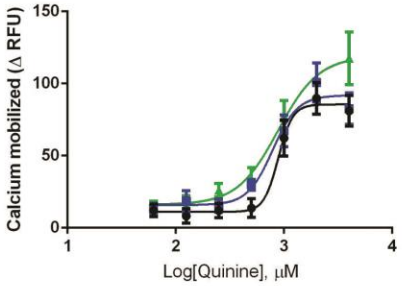
Calcium mobilized (Δ RFU)
Log[Quinine], μM
WT-T2R7
T255A
T255S

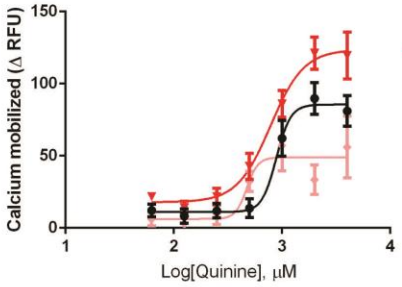
Calcium mobilized (Δ RFU)
Log[Quinine], μM
WT-T2R7
E271A
E271D

Figure 19 Concentration-dependent calcium response of T2R7 and mutants treated with quinine. Cells transiently transfected with WT-T2R7 or mutants in pcDNA3.1 were treated with different concentrations of quinine ranging from 0.0625 to 4 mM. Calcium mobilized (change in relative fluorescence units or ΔRFU) in each assay is shown after subtracting the baseline response of mock-transfected cells (pcDNA 3.1 transfected cells). EC_{50} values were determined by nonlinear regression analysis using PRISM software version 6.01 (GraphPad Software Inc., San Diego, CA). The results are from a minimum of n=3 independent experiments with each data point in triplicate.

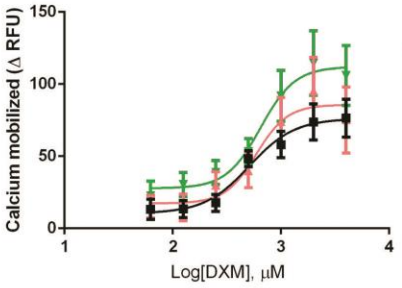
Calcium mobilized (Δ RFU)
150
100
50
0
1
2
3
4
Log[DXM], μM
WT
D65A
D65E

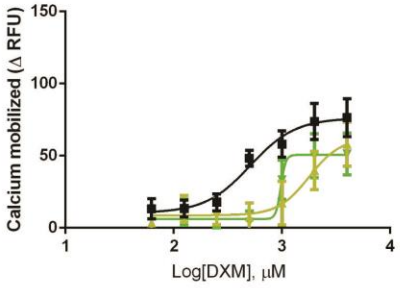
Calcium mobilized (Δ RFU)
150
100
50
0
1
2
3
4
Log[DXM], μM
WT
D86A
D86E

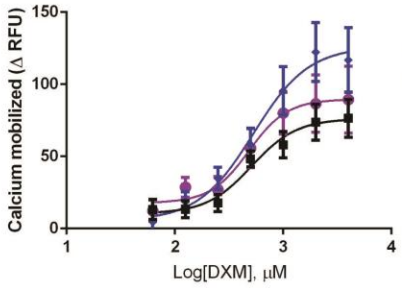
Calcium mobilized (Δ RFU)
150
100
50
0
1
2
3
4
Log[DXM], μM
WT
W89A
W89H

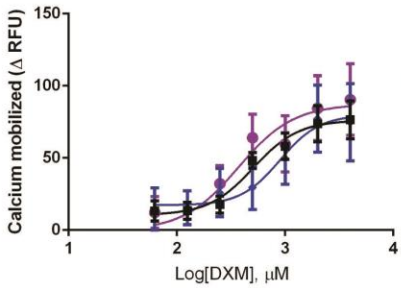
Calcium mobilized (Δ RFU)
150
100
50
0
1
2
3
4
Log[DXM], μM
WT
N167A
N167Q

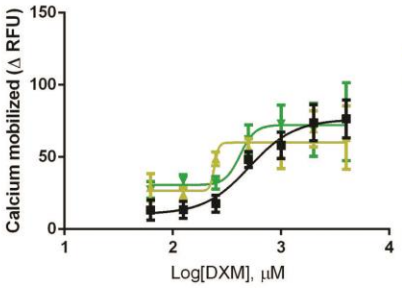
Calcium mobilized (Δ RFU)
150
100
50
0
1
2
3
4
Log[DXM], μM
WT
T169A
T169S

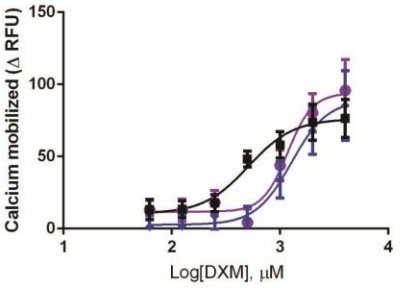
Calcium mobilized (Δ RFU)
150
100
50
0
1
2
3
4
Log[DXM], μM
WT
W170A
W170H

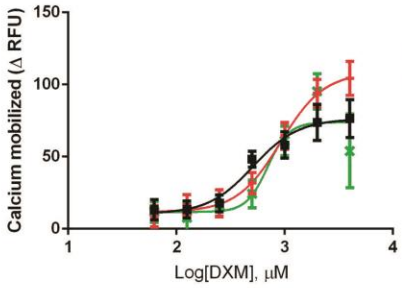
Calcium mobilized (Δ RFU)
150
100
50
0
1
2
3
4
Log[DXM], μM
WT
S181A
S181T

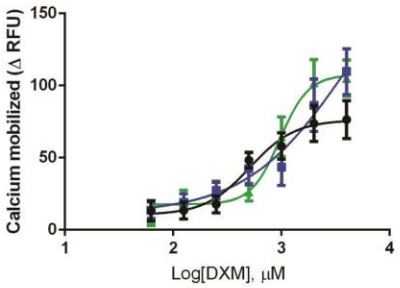
Calcium mobilized (Δ RFU)
150
100
50
0
1
2
3
4
Log[DXM], μM
WT-T2R7
T255A
T255S

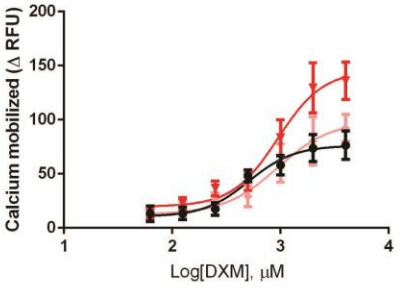
Calcium mobilized (Δ RFU)
200
150
100
50
0
1
2
3
4
Log[DXM], μM
WT-T2R7
E271A
E271D

Figure 20 Concentration-dependent calcium response of T2R7 mutants treated with dextromethorphan. Cells transiently transfected with WT-T2R7 or mutants in pcDNA3.1 were treated with different concentrations of dextromethorphan (DXM) ranging from 0.0625 to 4 mM. Calcium mobilized (ΔRFU) in each assay is shown after subtracting the baseline response of mock-transfected HEK293T cells (pcDNA 3.1 transfected cells). EC_{50} values were determined by nonlinear regression analysis using PRISM software version 6.01 (GraphPad Software Inc., San Diego, CA). The results are from a minimum of n=3 independent experiments with each data point in triplicate.

Table 3 Pharmacological profile of T2R7 and mutants treated with quinine.

T2R7 WT or mutants	Quinine			Cell surface expression (MFI)
	EC_{50} (μM)	EC_{50} Mutant/WT	E_{max} (ΔRFU)	
WT	888 ± 75		90 ± 11	2249 ± 412
D65A	662 ± 163	0.745	102 ± 19	2638 ± 325
D65E	626 ± 107	0.705	114 ± 8	2992 ± 562
D86A	1707 ± 260	1.921	116 ± 25	3062 ± 408
D86E	1595 ± 423	1.796	117 ± 31	2306 ± 681
W89A	715 ± 73	0.805	124 ± 9	2997 ±363
W89H	862 ± 179	0.971	97 ± 35	2524 ± 356
N167A	1108 ± 55	1.247	107 ± 24	2289 ± 432
N167Q	796 ± 101	0.896	97 ± 20	2078 ± 08
T169A	670 ± 115	0.753	111 ± 14	2713 ± 559
T169S	692 ± 275	0.778	105 ± 19	2791 ± 732
W170A	Not saturated		72 ± 31	2872 ± 473
W170H	Not saturated		91 ± 32	2806 ± 400
S181A	1433 ± 171	1.612	73 ± 25	2835 ± 592
S181T	Not determined		73 ± 15	2647 ± 281
T255A	795 ± 125	0.895	101 ± 14	2426 ± 544
T255S	881 ± 95	0.992	118 ± 18	2493 ± 152
E271A	786 ± 61	0.888	121 ± 11	2421 ± 301
E271D	562 ± 303	0.633	56 ± 21	2642 ± 52

Not saturated – No saturation of the calcium signal was observed even at the highest concentrations of the compound.
Not determined – The EC_{50} could not be determined under the assay conditions
Cell surface expression - measured by flow cytometry and represented as MFI (mock value from pcDNA3.1 transfected cells was deducted).

Table 4 Pharmacological profile of T2R7 and mutants treated with dextromethorphan.

T2R7 WT or mutants	Dextromethorphan			Cell surface expression (MFI)
	EC_{50} (μM)	EC_{50} Mutant/WT	E_{max} (ΔRFU)	
WT	519 ± 93		76 ± 13	2249 ± 412
D65A	608 ± 140	1.172	95 ± 23	2638 ± 325
D65E	655 ± 88	1.262	115 ± 22	2992 ± 562
D86A	1816 ±323	3.499	58 ± 15	3062 ± 408
D86E	Not determined		51 ±15	2306 ± 681
W89A	538 ± 86	1.037	122 ± 20	2997 ±363
W89H	487 ± 76	0.938	89 ± 23	2524 ± 356
N167A	911 ± 167	1.755	77 ± 23	2289 ± 432
N167Q	410 ± 176	0.790	91 ± 25	2078 ± 08
T169A	Not determined		70 ±12	2713 ± 559
T169S	423 ± 59	0.815	75 ± 27	2791 ± 732
W170A	1285 ± 118	2.476	86 ± 24	2872 ± 473
W170H	1187 ± 169	2.288	96 ± 22	2806 ± 400
S181A	920 ± 62	1.774	104 ± 12	2835 ± 592
S181T	745 ±258	1.436	95 ± 12	2647 ± 281
T255A	Not saturated		110 ± 16	2426 ± 544
T255S	974 ± 120	1.876	105 ± 13	2493 ± 152
E271A	957 ± 156	1.844	136 ± 17	2421 ± 301
E271D	956 ± 161	1.842	92 ± 12	2642 ± 52

Not saturated – No saturation of the calcium signal was observed even at the highest concentrations of the compound.
Not determined – The EC_{50} could not be determined under the assay conditions
Cell surface expression - measured by flow cytometry and represented as MFI (mock value from pcDNA3.1 transfected cells was deducted).

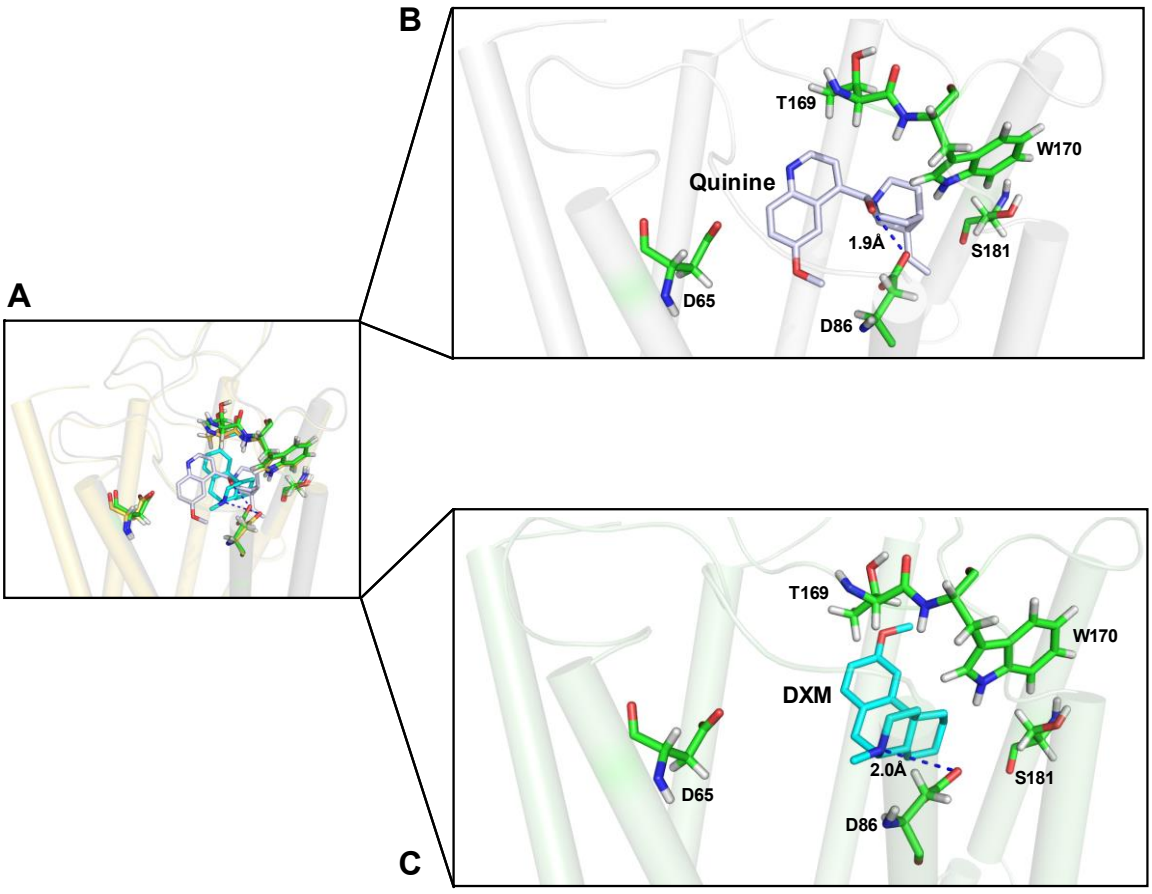

Figure 21 Molecular model of T2R7 bound to quinine and dextromethorphan (DXM). **A.** Overlay of T2R7 bound to both quinine (gray) and DXM (cyan). **B and C.** Inset panels showing T2R7 bound to quinine (**B**) and DXM (**C**) and the amino acids within 4Å region or interacting with the ligands. Quinine appears bound deeper compared to DXM within the T2R7 ligand binding pocket.

CHAPTER 5

DISCUSSION AND FUTURE DIRECTIONS

5.1 T2R7 ligand screening and characterization

Screening of ligands for T2R7 in this study, led to the identification of novel compounds that activate T2R7, while some previously reported T2R7 agonists did not produce a functional response in cells expressing the T2R7 receptor. Among the previously reported T2R7 agonists, no functional T2R7 response was observed upon treatment with chloroquine, cromolyn and malvidin-3-glucoside. Several compounds including dextromethorphan, diphenhydramine, thiamine, tobramycin and erythromycin were found to be novel ligands of the T2R7 receptor. .

Quinine, a medication for malaria treatment, has been reported to activate multiple T2Rs (Meyerhof 2010, Upadhyaya 2016). It is also reported to have pharmacochaperone activity on T2Rs as it increases the cell surface expression for several T2Rs including T2R7 (Upadhyaya 2016). In this study, quinine caused a robust increase in intracellular calcium mobilization in T2R7 expressing HEK293T stable cells with a maximum agonist effect (E_{max}) of 133 ± 15 ΔRFU. The EC_{50} value of quinine for T2R7 was found to be 906 ± 432 μM. These values are within the range for WT-T2R7 observed from transiently transfected cells. As it was previously reported that quinine treatment (incubation with 1 mM quinine for 1 hour at 37°C) causes a ~3-fold increase in cell surface expression of T2R7 expressed heterologously in HEK293T cells, in future studies, the mechanism of quinine promoting T2R7 expression can be further pursued. Whether T2R7 is involved in the side effects of quinine (such as headache, visual disorders, and sweating) as a malaria treatment also remains to be investigated.

Dextromethorphan and diphenhydramine were not reported as T2R7 agonists previously, however in this study they caused activation of T2R7. The E_{max} values for dextromethorphan and diphenhydramine are 81 $\pm$ 12 ΔRFU and 111 ± 17 ΔRFU, respectively. The EC_{50} values for dextromethorphan and diphenhydramine are 343 ± 57 μM and 414 ± 67 μM respectively, making these two compounds potent T2R7 agonists. Two structurally unrelated antibiotics, tobramycin (aminoglucoside) and erythromycin (macrolide) showed a modest activation of T2R7. The aminoglycoside, tobramycin is prescribed for treating *Pseudomonas aeruginosa* infections primarily in cystic fibrosis, while erythromycin is prescribed for many bacterial infections like skin and respiratory tract infections. As T2Rs are expressed in many extraoral tissues, whether antibiotics acting through T2Rs might cause additional and unintended effects remains to be studied.

5.2 Beef protein hydrolysates as a source of T2R ligands

Peptides as T2R ligands are of great importance, as many peptides are bioactive and they comprise an important part of human diet. In this study, beef protein hydrolysates were investigated for their ability to activate or inactivate T2R7. Results showed that all four peaks from alcalase fraction one (A1P1 to A1P4) and two peaks from chymotrypsin fraction four (C4P3 and C4P6) showed T2R7 blocking effects. As these fractions contain a variety of different peptides, LC-MS/MS should be pursued to obtain the sequences of the peptides in these mixtures, and each peptide should be tested on T2R7 stable cell line to further characterize these ligands. There are more than a hundred compounds (natural and synthetic) that have been reported to activate T2Rs, while only few blockers have been identified (Jaggupilli 2016). The pharmacological profile (antagonism) of these peptides

from beef protein hydrolysates needs to be characterized on multiple T2Rs, in addition to T2R7. This would determine whether these peptides have narrow or broad T2R blocking specificity. If the identified peptides have broad specificity as T2R blockers (i.e., blocking the majority of the 25 T2Rs in humans), they will have immense potential that will range from including them as flavour or food additives to improving the palatability of liquid medications and bitter tasting healthy foods. In addition, narrow or T2R specific peptide blockers will have potential use as pharmacological inhibitors to study the physiology of specific T2Rs expressed in extraoral tissues.

5.3 Ligand binding pocket of T2R7

There is no crystal structure available for any T2R. In order to study structure-function relationships of T2Rs, computational 3D models combined with mutational experiments are widely used. Previous studies have reached a consensus that ECL regions and extracellular TM regions interact with ligands, while the TM core maintains the receptor structure and ICL regions activate G proteins (reviewed by (Jaggupilli 2016)). In this study, a 3D homology model of T2R7 was built and this model was docked with two T2R7 agonists (quinine and dextromethorphan) with different efficacies. The docking results were analyzed with a focus on T2R7 residues that might contribute to the observed differences towards quinine and dextromethorphan binding. Nine amino acid residues in T2R7 including D65, D86, W89, N167, T169, W170, S181, T255 and E271 were selected for site-directed mutagenesis. These residues are located on the extracellular side of TM2, TM3, TM6, TM7, and ECL2 of T2R7, as shown in Figure 17.

Majority of the mutants were properly expressed on the cell surface as determined by flow cytometry. Based on the mutational results, the residues can be classified into two groups based on affinity for a particular ligand. The first group includes essential residues important for ligand binding and these are D86, W170 and S181. Mutation of these residues significantly reduces the ability of T2R7 to bind ligand and this is independent of the type of ligand. The second group includes residues that are ligand specific like D65 and W89 for quinine. These residues enhance binding to a specific category of ligands, and their mutation influences the ability of T2R7 to bind only those ligands.

Interestingly, no significant differences in pharmacological characteristics are observed between alanine and conservative substitutions at most positions. Furthermore, all of these positions are present on the extracellular surface of TMs or on ECL2. This suggests that the function of the amino acid at these positions is dictated by multiple factors that include the type of ligand, and the movements in TMs and ECL2 to accommodate the ligand. A recent 1μs molecular simulation study on T2R46 suggests the presence of a "vestibular site", which is more extracellular compared to a traditional buried orthosteric site (Sandal 2015). While molecular simulations were not pursued in this study the extracellular location of both the bound ligands in T2R7 suggests a similar vestibular site.

This study identified the important role played by ECL2 in T2R ligand binding and activation. The glycosylation status of T2R7 remains to be determined. However, mutation of the possible N-glycosylated residue, N167 did not lead to significant changes in receptor expression though slightly altered ligand affinity. Molecular dynamic simulations might shed more light on the role of ECL2 in T2R7 activation.

CHAPTER SIX

REFERENCES

Adler, E., M. A. Hoon, K. L. Mueller, J. Chandrashekar, N. J. Ryba and C. S. Zuker (2000). "A novel family of mammalian taste receptors." Cell **100**(6): 693-702.

Akabas, M. H., J. Dodd and Q. Al-Awqati (1988). "A bitter substance induces a rise in intracellular calcium in a subpopulation of rat taste cells." Science **242**(4881): 1047-1050.

Bachmanov, A. A. and G. K. Beauchamp (2007). "Taste receptor genes." Annu Rev Nutr **27**: 389-414.

Barlow, L. A. (2015). "Progress and renewal in gustation: new insights into taste bud development." Development **142**(21): 3620-3629.

Behrens, M., W. Meyerhof, C. Hellfritsch and T. Hofmann (2011). "Sweet and umami taste: natural products, their chemosensory targets, and beyond." Angew Chem Int Ed Engl **50**(10): 2220-2242.

Canessa, C. M., L. Schild, G. Buell, B. Thorens, I. Gautschi, J. D. Horisberger and B. C. Rossier (1994). "Amiloride-sensitive epithelial Na+ channel is made of three homologous subunits." Nature **367**(6462): 463-467.

Chakraborty, R., B. Xu, R. P. Bhullar and P. Chelikani (2015). "Expression of G protein-coupled receptors in Mammalian cells." Methods Enzymol **556**: 267-281.

Chandrashekar, J., M. A. Hoon, N. J. Ryba and C. S. Zuker (2006). "The receptors and cells for mammalian taste." Nature **444**(7117): 288-294.

Chandrashekar, J., K. L. Mueller, M. A. Hoon, E. Adler, L. Feng, W. Guo, C. S. Zuker and N. J. Ryba (2000). "T2Rs function as bitter taste receptors." Cell **100**(6): 703-711.

Chandrashekar, J., K. L. Mueller, M. A. Hoon, E. Adler, L. X. Feng, W. Guo, C. S. Zuker and N. J. P. Ryba (2000). "T2Rs function as bitter taste receptors." Cell **100**(6): 703-711.

Chandrashekar, J., D. Yarmolinsky, L. von Buchholtz, Y. Oka, W. Sly, N. J. Ryba and C. S. Zuker (2009). "The taste of carbonation." Science **326**(5951): 443-445.

Chaudhari, N. and S. D. Roper (2010). "The cell biology of taste." J Cell Biol **190**(3): 285-296.

Clark, A. A., C. D. Dotson, A. E. Elson, A. Voigt, U. Boehm, W. Meyerhof, N. I. Steinle and S. D. Munger (2015). "TAS2R bitter taste receptors regulate thyroid function." FASEB J **29**(1): 164-172.

Clark, A. A., S. B. Liggett and S. D. Munger (2012). "Extraoral bitter taste receptors as mediators of off-target drug effects." FASEB J **26**(12): 4827-4831.

Conte, C., M. Ebeling, A. Marcuz, P. Nef and P. J. Andres-Barquin (2002). "Identification and characterization of human taste receptor genes belonging to the TAS2R family." Cytogenet Genome Res **98**(1): 45-53.

Daoudi, H., J. Plesnik, A. Sayed, O. Sery, A. Rouabah, L. Rouabah and N. A. Khan (2015). "Oral Fat Sensing and CD36 Gene Polymorphism in Algerian Lean and Obese Teenagers." Nutrients **7**(11): 9096-9104.

DeFazio, R. A., G. Dvoryanchikov, Y. Maruyama, J. W. Kim, E. Pereira, S. D. Roper and N. Chaudhari (2006). "Separate populations of receptor cells and presynaptic cells in mouse taste buds." J Neurosci **26**(15): 3971-3980.

Delay, R. J., J. C. Kinnamon and S. D. Roper (1986). "Ultrastructure of mouse vallate taste buds: II. Cell types and cell lineage." J Comp Neurol **253**(2): 242-252.

Deshpande, D. A., W. C. Wang, E. L. McIlmoyle, K. S. Robinett, R. M. Schillinger, S. S. An, J. S. Sham and S. B. Liggett (2010). "Bitter taste receptors on airway smooth muscle bronchodilate by localized calcium signaling and reverse obstruction." Nat Med **16**(11): 1299-1304.
Finger, T. E. (2005). "Cell types and lineages in taste buds." Chem Senses **30 Suppl 1**: i54-55.
Finger, T. E., V. Danilova, J. Barrows, D. L. Bartel, A. J. Vigers, L. Stone, G. Hellekant and S. C. Kinnamon (2005). "ATP signaling is crucial for communication from taste buds to gustatory nerves." Science **310**(5753): 1495-1499.
Foster, S. R., E. R. Porrello, B. Purdue, H. W. Chan, A. Voigt, S. Frenzel, R. D. Hannan, K. M. Moritz, D. G. Simmons, P. Molenaar, E. Roura, U. Boehm, W. Meyerhof and W. G. Thomas (2013). "Expression, Regulation and Putative Nutrient-Sensing Function of Taste GPCRs in the Heart." Plos One **8**(5).
Fredriksson, R., M. C. Lagerstrom, L. G. Lundin and H. B. Schioth (2003). "The G-protein-coupled receptors in the human genome form five main families. Phylogenetic analysis, paralogon groups, and fingerprints." Mol Pharmacol **63**(6): 1256-1272.
Fuqua, W. C., S. C. Winans and E. P. Greenberg (1994). "Quorum sensing in bacteria: the LuxR-LuxI family of cell density-responsive transcriptional regulators." J Bacteriol **176**(2): 269-275.
Girgih, A. T., C. C. Udenigwe and R. E. Aluko (2013). "Reverse-phase HPLC separation of hemp seed (Cannabis sativa L.) protein hydrolysate produced peptide fractions with enhanced antioxidant capacity." Plant Foods Hum Nutr **68**(1): 39-46.
Hoon, M. A., E. Adler, J. Lindemeier, J. F. Battey, N. J. Ryba and C. S. Zuker (1999). "Putative mammalian taste receptors: a class of taste-specific GPCRs with distinct topographic selectivity." Cell **96**(4): 541-551.
Hughes, D. T. and V. Sperandio (2008). "Inter-kingdom signalling: communication between bacteria and their hosts." Nat Rev Microbiol **6**(2): 111-120.
Jaggupilli, A., R. Howard, J. D. Upadhyaya, R. P. Bhullar and P. Chelikani (2016). "Bitter taste receptors: Novel insights into the biochemistry and pharmacology." Int J Biochem Cell Biol **77**(Pt B): 184-196.
Ji, M., X. Su, X. Su, Y. Chen, W. Huang, J. Zhang, Z. Gao, C. Li and X. Lu (2014). "Identification of novel compounds for human bitter taste receptors." Chem Biol Drug Des **84**(1): 63-74.
Kenakin, T. (2004). "Principles: receptor theory in pharmacology." Trends Pharmacol Sci **25**(4): 186-192.
Kim, H. O. and E. C. Li-Chan (2006). "Quantitative structure-activity relationship study of bitter peptides." J Agric Food Chem **54**(26): 10102-10111.
Kimball, B. A., D. L. Nolte and K. B. Perry (2005). "Hydrolyzed casein reduces browsing of trees and shrubs by white-tailed deer." Hortscience **40**(6): 1810-1814.
Laskowski, R. A., J. A. Rullmannn, M. W. MacArthur, R. Kaptein and J. M. Thornton (1996). "AQUA and PROCHECK-NMR: programs for checking the quality of protein structures solved by NMR." J Biomol NMR **8**(4): 477-486.
Laugerette, F., P. Passilly-Degrace, B. Patris, I. Niot, M. Febbraio, J. P. Montmayeur and P. Besnard (2005). "CD36 involvement in orosensory detection of dietary lipids, spontaneous fat preference, and digestive secretions." J Clin Invest **115**(11): 3177-3184.
Lawton, D. M., D. N. Furness, B. Lindemann and C. M. Hackney (2000). "Localization of the glutamate-aspartate transporter, GLAST, in rat taste buds." Eur J Neurosci **12**(9): 3163-3171.
Le Neve, B., M. Foltz, H. Daniel and R. Gouka (2010). "The steroid glycoside H.g.-12 from Hoodia gordonii activates the human bitter receptor TAS2R14 and induces CCK release from HuTu-80 cells." Am J Physiol Gastrointest Liver Physiol **299**(6): G1368-1375.
Lee, R. J., G. Xiong, J. M. Kofonow, B. Chen, A. Lysenko, P. Jiang, V. Abraham, L. Doghramji, N. D. Adappa, J. N. Palmer, D. W. Kennedy, G. K. Beauchamp, P. T. Doulias, H. Ischiropoulos, J. L.

Kreindler, D. R. Reed and N. A. Cohen (2012). "T2R38 taste receptor polymorphisms underlie susceptibility to upper respiratory infection." J Clin Invest **122**(11): 4145-4159.
Leguebe, M., C. Nguyen, L. Capece, Z. Hoang, A. Giorgetti and P. Carloni (2012). "Hybrid molecular mechanics/coarse-grained simulations for structural prediction of G-protein coupled receptor/ligand complexes." PLoS One **7**(10): e47332.
Li, F. and M. Zhou (2012). "Depletion of bitter taste transduction leads to massive spermatid loss in transgenic mice." Mol Hum Reprod **18**(6): 289-297.
Li, X., L. Staszewski, H. Xu, K. Durick, M. Zoller and E. Adler (2002). "Human receptors for sweet and umami taste." Proc Natl Acad Sci U S A **99**(7): 4692-4696.
Liu, Y. Q., P. Strappe, W. T. Shang and Z. K. Zhou (2017). "Functional peptides derived from rice bran proteins." Crit Rev Food Sci Nutr: 0.
Lund, T. C., A. J. Kobs, A. Kramer, M. Nyquist, M. T. Kuroki, J. Osborn, D. S. Lidke, S. T. Low-Nam, B. R. Blazar and J. Tolar (2013). "Bone marrow stromal and vascular smooth muscle cells have chemosensory capacity via bitter taste receptor expression." PLoS One **8**(3): e58945.
Maehashi, K. and L. Huang (2009). "Bitter peptides and bitter taste receptors." Cell Mol Life Sci **66**(10): 1661-1671.
Maehashi, K., M. Matano, H. Wang, L. A. Vo, Y. Yamamoto and L. Huang (2008). "Bitter peptides activate hTAS2Rs, the human bitter receptors." Biochem Biophys Res Commun **365**(4): 851-855.
Marchiori, A., L. Capece, A. Giorgetti, P. Gasparini, M. Behrens, P. Carloni and W. Meyerhof (2013). "Coarse-grained/molecular mechanics of the TAS2R38 bitter taste receptor: experimentally-validated detailed structural prediction of agonist binding." PLoS One **8**(5): e64675.
Matsunami, H., J. P. Montmayeur and L. B. Buck (2000). "A family of candidate taste receptors in human and mouse." Nature **404**(6778): 601-604.
Mattes, R. D. (2001). "The taste of fat elevates postprandial triacylglycerol." Physiol Behav **74**(3): 343-348.
Maurer, S., G. H. Wabnitz, N. A. Kahle, S. Stegmaier, B. Prior, T. Giese, M. M. Gaida, Y. Samstag and G. M. Hansch (2015). "Tasting Pseudomonas aeruginosa Biofilms: Human Neutrophils Express the Bitter Receptor T2R38 as Sensor for the Quorum Sensing Molecule N-(3-Oxododecanoyl)-l-Homoserine Lactone." Front Immunol **6**: 369.
Meyerhof, W., C. Batram, C. Kuhn, A. Brockhoff, E. Chudoba, B. Bufe, G. Appendino and M. Behrens (2010). "The molecular receptive ranges of human TAS2R bitter taste receptors." Chem Senses **35**(2): 157-170.
Miguel, M., R. Lopez-Fandino, M. Ramos and A. Aleixandre (2005). "Short-term effect of egg-white hydrolysate products on the arterial blood pressure of hypertensive rats." Br J Nutr **94**(5): 731-737.
Mirzapour, M., K. Rezaei and M. A. Sentandreu (2017). "Identification of Potent ACE Inhibitory Peptides from Wild Almond Proteins." J Food Sci.
Nakamura, Y., N. Yamamoto, K. Sakai and T. Takano (1995). "Antihypertensive effect of sour milk and peptides isolated from it that are inhibitors to angiotensin I-converting enzyme." J Dairy Sci **78**(6): 1253-1257.
Nelson, G., M. A. Hoon, J. Chandrashekar, Y. Zhang, N. J. Ryba and C. S. Zuker (2001). "Mammalian sweet taste receptors." Cell **106**(3): 381-390.
Nelson, G. M. and T. E. Finger (1993). "Immunolocalization of different forms of neural cell adhesion molecule (NCAM) in rat taste buds." J Comp Neurol **336**(4): 507-516.
Pin, J. P., T. Galvez and L. Prezeau (2003). "Evolution, structure, and activation mechanism of family 3/C G-protein-coupled receptors." Pharmacol Ther **98**(3): 325-354.

Pydi, S. P., N. Singh, J. Upadhyaya, R. P. Bhullar and P. Chelikani (2014). "The third intracellular loop plays a critical role in bitter taste receptor activation." Biochim Biophys Acta **1838**(1 Pt B): 231-236.
Pydi, S. P., T. Sobotkiewicz, R. Billakanti, R. P. Bhullar, M. C. Loewen and P. Chelikani (2014). "Amino acid derivatives as bitter taste receptor (T2R) blockers." J Biol Chem **289**(36): 25054-25066.
Rauh, V. M., L. B. Johansen, R. Ipsen, M. Paulsson, L. B. Larsen and M. Hammershoj (2014). "Plasmin activity in UHT milk: relationship between proteolysis, age gelation, and bitterness." J Agric Food Chem **62**(28): 6852-6860.
Reichling, C., W. Meyerhof and M. Behrens (2008). "Functions of human bitter taste receptors depend on N-glycosylation." J Neurochem **106**(3): 1138-1148.
Sainz, E., M. M. Cavenagh, J. Gutierrez, J. F. Battey, J. K. Northup and S. L. Sullivan (2007). "Functional characterization of human bitter taste receptors." Biochem J **403**(3): 537-543.
Saito, Y., K. Wanezaki, A. Kawato and S. Imayasu (1994). "Structure and activity of angiotensin I converting enzyme inhibitory peptides from sake and sake lees." Biosci Biotechnol Biochem **58**(10): 1767-1771.
Sandal, M., M. Behrens, A. Brockhoff, F. Musiani, A. Giorgetti, P. Carloni and W. Meyerhof (2015). "Evidence for a Transient Additional Ligand Binding Site in the TAS2R46 Bitter Taste Receptor." J Chem Theory Comput **11**(9): 4439-4449.
Sato, J., N. Makita and T. Iiri (2016). "Inverse agonism: the classic concept of GPCRs revisited [Review]." Endocr J **63**(6): 507-514.
Seifert, R. and K. Wenzel-Seifert (2002). "Constitutive activity of G-protein-coupled receptors: cause of disease and common property of wild-type receptors." Naunyn Schmiedebergs Arch Pharmacol **366**(5): 381-416.
Sergi, G., G. Bano, S. Pizzato, N. Veronese and E. Manzato (2017). "Taste loss in the elderly: Possible implications for dietary habits." Crit Rev Food Sci Nutr **57**(17): 3684-3689.
Shah, A. S., Y. Ben-Shahar, T. O. Moninger, J. N. Kline and M. J. Welsh (2009). "Motile cilia of human airway epithelia are chemosensory." Science **325**(5944): 1131-1134.
Shaik, F. A., N. Singh, M. Arakawa, K. Duan, R. P. Bhullar and P. Chelikani (2016). "Bitter taste receptors: Extraoral roles in pathophysiology." Int J Biochem Cell Biol **77**(Pt B): 197-204.
Simon, S. A., I. E. de Araujo, R. Gutierrez and M. A. Nicolelis (2006). "The neural mechanisms of gustation: a distributed processing code." Nat Rev Neurosci **7**(11): 890-901.
Singh, N., R. Chakraborty, R. P. Bhullar and P. Chelikani (2014). "Differential expression of bitter taste receptors in non-cancerous breast epithelial and breast cancer cells." Biochem Biophys Res Commun **446**(2): 499-503.
Singh, N., M. Vrontakis, F. Parkinson and P. Chelikani (2011). "Functional bitter taste receptors are expressed in brain cells." Biochem Biophys Res Commun **406**(1): 146-151.
Smith, D. V., S. J. John and J. D. Boughter (2000). "Neuronal cell types and taste quality coding." Physiol Behav **69**(1-2): 77-85.
Smith, D. V. and S. J. St John (1999). "Neural coding of gustatory information." Curr Opin Neurobiol **9**(4): 427-435.
Soares, S., S. Kohl, S. Thalmann, N. Mateus, W. Meyerhof and V. De Freitas (2013). "Different phenolic compounds activate distinct human bitter taste receptors." J Agric Food Chem **61**(7): 1525-1533.
Spielman, A. I., T. Huque, H. Nagai, G. Whitney and J. G. Brand (1994). "Generation of inositol phosphates in bitter taste transduction." Physiol Behav **56**(6): 1149-1155.

Spielman, A. I., H. Nagai, G. Sunavala, M. Dasso, H. Breer, I. Boekhoff, T. Huque, G. Whitney and J. G. Brand (1996). "Rapid kinetics of second messenger production in bitter taste." Am J Physiol **270**(3 Pt 1): C926-931.
Suess, B., A. Brockhoff, W. Meyerhof and T. Hofmann (2016). "The Odorant (R)-Citronellal Attenuates Caffeine Bitterness by Inhibiting the Bitter Receptors TAS2R43 and TAS2R46." J Agric Food Chem.
Temussi, P. A. (2009). "Sweet, bitter and umami receptors: a complex relationship." Trends Biochem Sci **34**(6): 296-302.
Thomas, A., C. Sulli, E. Davidson, E. Berdougo, M. Phillips, B. A. Puffer, C. Paes, B. J. Doranz and J. B. Rucker (2017). "The Bitter Taste Receptor TAS2R16 Achieves High Specificity and Accommodates Diverse Glycoside Ligands by using a Two-faced Binding Pocket." Sci Rep **7**(1): 7753.
Tizzano, M., B. D. Gulbransen, A. Vandenbeuch, T. R. Clapp, J. P. Herman, H. M. Sibhatu, M. E. A. Churchill, W. L. Silver, S. C. Kinnamon and T. E. Finger (2010). "Nasal chemosensory cells use bitter taste signaling to detect irritants and bacterial signals." Proceedings of the National Academy of Sciences of the United States of America **107**(7): 3210-3215.
Upadhyaya, J., S. P. Pydi, N. Singh, R. E. Aluko and P. Chelikani (2010). "Bitter taste receptor T2R1 is activated by dipeptides and tripeptides." Biochem Biophys Res Commun **398**(2): 331-335.
Upadhyaya, J. D., R. Chakraborty, F. A. Shaik, A. Jaggupilli, R. P. Bhullar and P. Chelikani (2016). "The Pharmacochaperone Activity of Quinine on Bitter Taste Receptors." PLoS One **11**(5): e0156347.
Upadhyaya, J. D., N. Singh, A. S. Sikarwar, R. Chakraborty, S. P. Pydi, R. P. Bhullar, S. Dakshinamurti and P. Chelikani (2014). "Dextromethorphan mediated bitter taste receptor activation in the pulmonary circuit causes vasoconstriction." PLoS One **9**(10): e110373.
Vroling, B., M. Sanders, C. Baakman, A. Borrmann, S. Verhoeven, J. Klomp, L. Oliveira, J. de Vlieg and G. Vriend (2011). "GPCRDB: information system for G protein-coupled receptors." Nucleic Acids Res **39**(Database issue): D309-319.
Wang, W. Y. and E. G. De Mejia (2005). "A new frontier in soy bioactive peptides that may prevent age-related chronic diseases." Comprehensive Reviews in Food Science and Food Safety **4**(4): 63-78.
Wiener, A., M. Shudler, A. Levit and M. Y. Niv (2012). "BitterDB: a database of bitter compounds." Nucleic Acids Res **40**(Database issue): D413-419.
Wolfle, U., F. A. Elsholz, A. Kersten, B. Haarhaus, W. E. Muller and C. M. Schempp (2015). "Expression and functional activity of the bitter taste receptors TAS2R1 and TAS2R38 in human keratinocytes." Skin Pharmacol Physiol **28**(3): 137-146.
Wong, G. T., K. S. Gannon and R. F. Margolskee (1996). "Transduction of bitter and sweet taste by gustducin." Nature **381**(6585): 796-800.
Wu, S. V., N. Rozengurt, M. Yang, S. H. Young, J. Sinnett-Smith and E. Rozengurt (2002). "Expression of bitter taste receptors of the T2R family in the gastrointestinal tract and enteroendocrine STC-1 cells." Proc Natl Acad Sci U S A **99**(4): 2392-2397.
Yang, R., H. H. Crowley, M. E. Rock and J. C. Kinnamon (2000). "Taste cells with synapses in rat circumvallate papillae display SNAP-25-like immunoreactivity." J Comp Neurol **424**(2): 205-215.
Zhao, C. J., A. Schieber and M. G. Ganzle (2016). "Formation of taste-active amino acids, amino acid derivatives and peptides in food fermentations - A review." Food Res Int **89**(Pt 1): 39-47.
Zheng, K., P. Lu, E. Delpapa, K. Bellve, R. Deng, J. C. Condon, K. Fogarty, L. M. Lifshitz, T. A. M. Simas, F. Shi and R. ZhuGe (2017). "Bitter taste receptors as targets for tocolytics in preterm labor therapy." FASEB J.